NASA/TM-20220002098

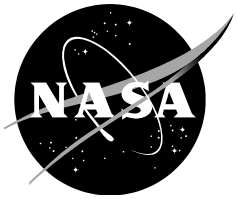

A Benchmark Example for Delamination Propagation Predictions Based on the Calibrated End-Loaded Split Specimen

Ronald Krueger
National Institute of Aerospace, Hampton, Virginia, USA

Nelson V. De Carvalho
NASA Langley Research Center, Hampton, Virginia, USA

February 2022

NASA STI Program Report Series

The NASA STI Program collects, organizes, provides for archiving, and disseminates NASA's STI. The NASA STI program provides access to the NTRS Registered and its public interface, the NASA Technical Reports Server, thus providing one of the largest collections of aeronautical and space science STI in the world. Results are published in both non-NASA channels and by NASA in the NASA STI Report Series, which includes the following report types:

- TECHNICAL PUBLICATION. Reports of completed research or a major significant phase of research that present the results of NASA Programs and include extensive data or theoretical analysis. Includes compilations of significant scientific and technical data and information deemed to be of continuing reference value. NASA counterpart of peer-reviewed formal professional papers but has less stringent limitations on manuscript length and extent of graphic presentations.

- TECHNICAL MEMORANDUM. Scientific and technical findings that are preliminary or of specialized interest, e.g., quick release reports, working papers, and bibliographies that contain minimal annotation. Does not contain extensive analysis.

- CONTRACTOR REPORT. Scientific and technical findings by NASA-sponsored contractors and grantees.

- CONFERENCE PUBLICATION. Collected papers from scientific and technical conferences, symposia, seminars, or other meetings sponsored or co-sponsored by NASA.

- SPECIAL PUBLICATION. Scientific, technical, or historical information from NASA programs, projects, and missions, often concerned with subjects having substantial public interest.

- TECHNICAL TRANSLATION. English-language translations of foreign scientific and technical material pertinent to NASA's mission.

Specialized services also include organizing and publishing research results, distributing specialized research announcements and feeds, providing information desk and personal search support, and enabling data exchange services.

For more information about the NASA STI program, see the following:

- Access the NASA STI program home page at http://www.sti.nasa.gov

- Help desk contact information:

https://www.sti.nasa.gov/sti-contact-form/ and select the "General" help request type.

NASA/TM–20220002098

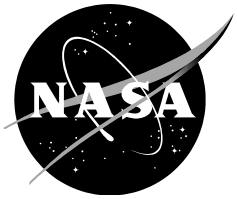

A Benchmark Example for Delamination Propagation Predictions Based on the Calibrated End-Loaded Split Specimen

Ronald Krueger
National Institute of Aerospace, Hampton, Virginia, USA

Nelson V. De Carvalho
NASA Langley Research Center, Hampton, Virginia, USA

National Aeronautics and
Space Administration

Langley Research Center
Hampton, VA 23681

February 2022

This report is available in electronic form at

http://

A Benchmark Example for Delamination Propagation Predictions Based on the Calibrated End-Loaded Split Specimen

Ronald Krueger
National Institute of Aerospace, Hampton, Virginia, USA

Nelson V. De Carvalho
NASA Langley Research Center, Hampton, Virginia, USA

ABSTRACT

A benchmark example based on the Calibrated End-Loaded Split (C-ELS) specimen is developed and used to assess the performance of recently developed delamination propagation capabilities in the Abaqus/Standard finite element code. The C-ELS specimen has the advantage of a longer region of stable delamination propagation compared to the existing mode II benchmark case. The new benchmark example may therefore provide a better assessment tool by enabling more stable crack growth in regions further away from the boundary conditions or load application. First, a benchmark result is created manually using two-dimensional finite element models of the C-ELS specimen with different delamination lengths. Second, the performance of the delamination propagation capabilities in the Abaqus/Standard finite element code are assessed by comparing the results to the benchmark case. Two examples with different starter delamination lengths are studied. A shorter starter length is chosen to create a scenario with unstable delamination propagation. A longer delamination causes stable delamination propagation. Detailed results from three-dimensional analyses with aligned and mis-aligned meshes and two levels of mesh refinement are provided for several permutations of numerical input parameters. In general, good agreement can be achieved between the results obtained from the quasi-static propagation analysis and the benchmark analysis. However, particular non-default settings are found to be most reliable, accurate, and numerically efficient. Numerical artifacts including anomalous unreleased nodes in the crack wake and zig-zag crack fronts occur, and further development of the Abaqus/Standard VCCT propagation may be required. Use of the benchmark case to assess the continuous improvements in one finite element code illustrates the value of establishing benchmark solutions.

INTRODUCTION

Over the past two decades, the use of fracture mechanics has become common practice to characterize the onset and growth of delaminations in laminated composites[1],[2]. In order to predict delamination onset or growth, the calculated strain energy release rate components are compared to interlaminar fracture toughness properties measured over a range from pure mode I loading to pure mode II loading [2].

The virtual crack closure technique (VCCT) is widely used for computing energy release rates based on results from continuum (2D) and solid (3D) finite element (FE) analyses, and to supply the mode separation required when using the mixed-mode fracture criterion [3],[4]. Recently, VCCT was implemented into several commercial finite element codes such as Abaqus/Standard®, Nastran™, Marc™, and Ansys®. As new methods for analyzing composite delamination are incorporated into finite element codes, the need for comparison and benchmarking becomes important, since each code requires specific input parameters unique to its implementation. In the context of analysis Verification and Validation (V&V) [5], these benchmarks may also be used for code and calculation verification purposes and thus serve as a valuable tool for software developers. Further, these benchmark solutions may be used to

evaluate other algorithms for delamination prediction, such as cohesive elements and adaptive mesh VCCT algorithms. Therefore, a software independent approach for benchmarking based on Linear Elastic Fracture Mechanics (LEFM) was recently presented and demonstrated for the implementation in Abaqus/Standard® [6]. The benchmark examples are based on two-dimensional (2D) and three-dimensional (3D) finite element models of the Double Cantilever Beam (DCB), End-Notched Flexure (ENF) and Mixed-Mode Bending (MMB) specimens. To allow further assessment, new benchmark examples based on the Single-Leg Bending (SLB) specimen were created for delaminations under mixed-mode conditions where the mode ratio is also dependent on the delamination length, *a* [7],[8]. The approach allows for the assessment of the mode I, II, and mixed-mode I and II, delamination propagation capabilities in commercial finite element codes under static loading. The capability of other codes was assessed in Refs. [9], [10]. The same approach was used for all of the assessments. First, benchmark results were created manually using the VCCT implementation in the software of interest. Second, using the implemented VCCT-based automated propagation analysis, a delamination in a finite element model was allowed to propagate. In general, good agreement between the results obtained from the automated FE propagation analysis and the benchmark results could be achieved when the appropriate input parameters were selected. Nevertheless, the benchmarks also helped to identify aspects that needed further study.

The objective of the present study is to create a new benchmark example for delamination propagation under mode II, and demonstrate the use of this benchmark case to assess the performance of automated crack propagation prediction capabilities in Abaqus/Standard [11]. These capabilities are VCCT-based and allow crack propagation between two user-defined surfaces into a predefined zone of initially-tied, coincident node-pairs which get successively released. This new benchmark example is thought to complement the existing benchmark case based on the mode II End-Notched Flexure test shown in Figure 1a [12],[13]. The new benchmark example is based on the mode II Calibrated End-Loaded Split (C-ELS) specimen shown in Figure 1b [14],[15],[16]. Both specimens initially exhibit unstable delamination propagation which adds to the complexity of the analysis. However, the C-ELS specimen has the advantage that the region of stable delamination propagation begins at $a/L > 0.55$, compared to the ENF specimen where $a/L > 0.7$ is required for stable propagation. The new benchmark example may therefore provide a better assessment tool by enabling more stable crack growth in regions further away from the boundary conditions or load application. Note that during unstable propagation, computed energy release rates that overshoot the fracture toughness may not manifest as an error. Furthermore, the challenge of obtaining a solution during unstable crack growth may hinder the assessment of other aspects of the algorithm. A larger region of stable propagation also enables assessment of the observations made in [13] and how they change when simulating stable delamination growth. For example, is the zig-zag front observed locally for unstable growth [13] caused by an increase in energy release rate with delamination length (positive dG/da)? The hypothesis is that after node release the new node at the locally advanced front experiences a higher energy release rate. Therefore, these new nodes would now be eligible to release rather than the neighboring nodes, causing the observed continued roughness across the width. Thus, a C-ELS specimen-based benchmark may offer the opportunity to study this hypothesis and overall may provide a better assessment tool.

In this paper, the development of a benchmark case based on the C-ELS specimen is presented. First, the development of a new VCCT-based benchmark case for crack propagation prediction under quasi-static loading is discussed in detail. Second, the application is demonstrated for the commercial finite element code Abaqus/Standard 2021 FD06[1]. Third,

[1] Improvements to the VCCT implementation in Abaqus/Standard are ongoing and more recent releases have additional functionality. All releases mentioned in this report are available to the public.

results obtained from VCCT-based, automated quasi-static propagation analysis are compared to the benchmark case. It was assumed that the computed behavior from accurate automated delamination propagation analyses should closely match the benchmark results. Lastly, the significance of the results is discussed.

ANALYSIS BENCHMARKING

The development of a benchmark case based on the C-ELS specimen is presented in the following section. First, the finite element models used for the benchmark creation and assessment are introduced. Second, the development of a new VCCT-based benchmark case for crack propagation prediction under quasi-static loading is presented in detail. Third, a comparison between load/displacement results and computed energy release rates obtained from 2D and 3D models is discussed. Finally, the automated VCCT-based delamination propagation analysis tool implemented in Abaqus/Standard is outlined.

Finite Element Model

For the current study, C-ELS specimens made of IM7/8552 graphite/epoxy were analyzed. The material properties were taken from a previous study [6]. Typical 2D and 3D models are shown on Figures 2 to 4. An example of the 2D FE model of the C-ELS specimens with boundary conditions is shown in Figure 2. Based on previous experience [6], the specimen was modeled with solid plane strain elements with incompatible modes (CPE4I) in Abaqus/Standard [11] to create the benchmark cases. The C-ELS specimen was modeled with six elements through the specimen thickness. Along the length, all models were divided into different sections with different mesh refinements. The element edge length at the delamination tip in the section of automated crack propagation was equal to 0.5 mm.

Examples of 3D finite element models of the C-ELS specimen are shown in Figure 3. Through the thickness and along the length, the 3D mesh was identical to the mesh described above for the 2D model. Across the width, a uniform mesh with ΔB=1mm element size, as shown in Figure 3a, was used to avoid potential problems at the transition between a coarse and finer mesh across the width. The specimen was modeled with solid brick elements with incompatible modes (C3D8I), which yielded excellent results in previous studies [6]. As in the 2D models, the model was divided into different sections with different mesh refinements along the length. A second 3D model with a refined mesh across the width with ΔB=0.5 mm element size, as shown in Figure 3b, was used for additional refinement studies.

For the VCCT analysis with Abaqus/Standard, the plane of delamination was modeled as a discrete discontinuity in the center of the specimen. The models were created as separate meshes for the upper and lower part of the specimens with identical nodal point coordinates in the plane of delamination. A top surface (magenta outline) and a bottom surface (bright green outline) were defined to specify the contact area in the plane of delamination, as shown in Figure 3a. Additionally, a node set (bonded nodes) was created to define the intact region (blue shaded area). The initial delamination front (dashed red line) defines the beginning of the intact region.

Additional models were created in which the element edges did not align with the advancing delamination front, as shown in Figure 4. This intentional misalignment was created as an extra challenge for the automated propagation analysis. It is expected that in more complex, large-scale problems where delamination initiation, size, and shape are unknown, it will not be possible to a priori align the mesh with the propagating front. It was thus deemed appropriate to evaluate the performance of a code for non-aligned meshes with an approach used previously [7]. Two meshes with ΔB=1mm and ΔB=0.5 mm element size across the width are shown in Figures 4a and 4b, respectively.

Development of Benchmark Case

Quasi-static benchmark results can easily be created for any FE analysis software used. The procedure is discussed in detail in a previous paper describing the benchmark creation [6] and is condensed here for brevity.

- First, finite element models of the specimen with different initial delamination lengths, a_0, are created. For the current example, two-dimensional finite element models simulating the C-ELS specimen were created with 20 different initial delamination lengths a_0 (50.0 mm ≤ a_0 ≤ 100.0 mm).
- For each a_0 modeled, the load, P, and end deflection, w, at the load point were plotted as shown in Figure 5, where each solid line represents a different value of a_0.
- For each a_0 modeled, the total strain energy release rate, G_T, and the mixed-mode ratio G_{II}/G_T were computed using VCCT for an applied tip deflection w =10.0 mm. In the current case, the mixed-mode ratio should theoretically be pure mode II (G_{II}/G_T=1) which will be verified later.
- For each a_0 modeled, a failure index, G_T/G_c, is calculated by comparing the computed total energy release rate, G_T, with the mixed-mode fracture toughness, G_c, of the material, often computed as a function of the mixed-mode ratio. When obtaining the benchmark, G_c should be determined using the same expression for G_c used later in the automated analysis. In the present study, the B-K criterion, suggested by Benzeggah and Kenane [17], was used. A BK-fit through experimental data for IM7/8552 is shown in Figure 6. Related fracture toughness data are presented in Table 2. It is assumed that the delamination propagates when the failure index reaches unity.
- Therefore, the critical load, P_c, and critical tip displacement, w_c, can be calculated based on the relationship between load, P, and the energy release rate, G, for a linear system:

$$\frac{G_T}{G_c} = \frac{P^2}{P_c^2} \Rightarrow P_c = P\sqrt{\frac{G_c}{G_T}}; \quad \text{and} \quad \frac{w_c}{2} = \frac{w}{2}\sqrt{\frac{G_c}{G_T}} \tag{1}$$

- For each delamination length, a_0, modeled, the critical load/displacement results were calculated using equation (1) and were included in the load/displacement plots as shown in Figure 7 (solid red circles)
- These critical load/displacement results indicated that, with increasing delamination length, less load is required to extend the delamination. For the first ten delamination lengths, a_0, investigated, the values of the critical displacements also decreased at the same time. This means that the C-ELS specimen exhibits unstable delamination propagation under load control as well as displacement control in this region. The remaining critical load/displacement results pointed to stable propagation.
  From these critical load/displacement results (dashed thin black line and solid circles), a benchmark solution (solid red line) can be created as shown in Figure 8. If the analysis is performed under displacement control (prescribed nodal displacements, w), the applied displacement must be held constant over several increments once the critical point (P_c, w_c) is reached, and the delamination front is advanced during these increments. Once the critical path is reached, the applied nodal displacement is increased again incrementally. For longer initial crack lengths (e.g. a_0 > 55 mm) stable propagation is expected throughout the entire analysis. During the automated propagation analysis, the computed load/displacement results are expected to follow the benchmark solution (solid red line). Throughout the development of the benchmark example using 2D models, it was assumed that the delamination front remained straight for each delamination length, a_0, modeled. In reality, however, a delamination front may develop into a somewhat curved front during propagation. This, however, was not

considered for the current benchmarking exercise. The following section provides evidence that a straight crack front is a reasonable assumption based on the computed energy release rate distributions across the width of the C-ELS specimen.

Computed load-displacement results obtained from 2D and 3D and models

A comparison of the load/displacement behavior of the C-ELS specimen computed from 2D models (open symbols and solid red lines) and 3D models (crosses and blue dashed lines) models is shown in Figure 9 for two different initial delamination lengths a_0 = 50 mm and 75 mm. Results indicate that the 2D and 3D models used have comparable stiffness. Thus, regarding the stiffness loss computed during automated delamination propagation, a comparison between results obtained using 3D models with the benchmark obtained from 2D analysis should be adequate.

Computed energy release rate distribution across the width of the specimen

The computed strain energy release rate values were plotted versus position along the width, B, of the C-ELS specimens, as shown in Figures 10 and 11. The results were obtained from models shown in Figure 2 for an applied tip displacement w = 10 mm for starter delamination lengths a_0 = 50 and 75 mm, respectively. The mode II strain energy release rate distribution (open blue squares and solid line) was found to be symmetric with respect to the center of the specimen and fairly constant over most of the width. The mode II contribution drops slightly towards the edges followed by a sudden peak close to the edges. Delamination propagation is expected to start at the edge but a fairly uniform straight front is expected to develop during propagation. The averaged value (dashed blue line) obtained from the 3D distribution compares well with the single result obtained from the 2D analyses (solid blue square). As expected, the mode I strain energy release rate was computed to be significantly smaller across the entire width of the specimen (solid red dots and line). The mode III strain energy release rate obtained from the 3D analyses were also several orders of magnitude smaller than the mode II values.

The increase of computed strain energy release rate values with increasing applied displacement is shown in Figures 12 and 13 for starter delamination lengths a_0 = 50 and 75 mm, respectively. Mode II results (blues lines) obtained from 2D analysis (solid symbols) and from 3D analysis averaged across the width (open symbols) are in good agreement. As expected, the mode I strain energy release rate remains small even with increasing displacement.

Results indicate that the 2D and 3D models yield comparable energy release rate results and in particular the 2D results are a good approximation of the averaged 3D results. Further, the energy release rate is fairly uniform over most of the width. Thus, based on the energy release rates computed during automated delamination propagation a comparison between results obtained using 3D models with the benchmark obtained from 2D analysis should be adequate.

Automated delamination propagation in Abaqus/Standard

The implementation of VCCT enables Abaqus to solve delamination problems in composite materials. The implementation is compatible with all the features in Abaqus such as large-scale nonlinear models of composite structures, including continuum shells, composite materials, cohesive elements, buckling, and contact. The plane of delamination in three-dimensional analyses is modeled using the existing crack propagation capability based on the contact pair capability. Additional element definitions are not required, and the underlying finite element mesh and model do not have to be modified [11]

In Abaqus/Standard, several input parameters control the analysis:

- The release tolerance parameter is used to improve the accuracy of the VCCT-based local solution [11]. If this release tolerance is exceeded in an increment ($(G-G_c)/G_c >$ *release tolerance*), a cutback operation is performed which reduces the time

increment. In the new smaller increment, the strain energy release rates are recalculated and compared to the user specified release tolerance. A release tolerance, *reltol*=0.2, is suggested in the handbook [11]. However, a tighter tolerance should be used to achieve better accuracy. For the current analysis, *reltol*=0.01 was chosen.

- Another parameter, which Abaqus/Standard provides to help overcome convergence issues during the propagation analysis, is *contact stabilization,* which is applied only across selected contact pairs and used to control the motion of two contact pairs while they approach each other in multi-body contact. Damping is applied when bonded contact pairs separate and move away from each other [11]. For the current analysis, a stabilization factor equal to 10^{-6}, which had yielded good results in previous analyses [6], was chosen. Excessive stabilization may adversely affect the predicted load levels.
- To simulate the propagation of cracks, the element at the crack tip may either be completely released once the fracture criterion is reached or released gradually. Abaqus/Standard offers the complete release using the option *debonding force=step* [11]. In contrast, a gradual release can be used to represent intermediate crack positions between existing node pairs. Using this approach, the nodes are allowed to be released progressively rather than suddenly and the forces are ramped down accordingly. Abaqus/Standard offers this approach using the option *debonding force=ramp* [11]. Both approaches were used in the current study and are referred to as *original input* in this report. More detailed information about VCCT with progressive nodal release can be found in a related paper [18].

Additional functionalities recommended by industry [19] regarding multi-node pair release during propagation and improved convergence algorithms, have become available in more recent Abaqus/Standard releases and are referred to as *new input* in this report. For an unstable crack growth problem, it is sometimes more efficient to allow multiple nodes at, and ahead of, a crack tip to release in one increment without cutting back the increment size.

- This capability is activated in Abaqus/Standard when an *unstable growth tolerance* is defined. If the fracture criterion is within the given *unstable growth tolerance,* the time increment size is reduced automatically to a very small value allowing more node pairs to release. Once the criterion is exceeded, the time increment size will be automatically recovered to a larger value to speed up the analysis [11]. The default value for unstable growth tolerance is infinity. Further, scaling parameters α and β (default α=0.5 and β=2.0*)* that influence the increment size and the recovery to a larger value after the unstable growth analysis may be defined to control the automated node release during automated propagation.
- An additional parameter *n* (default *n*=0) was introduced in Abaqus 2020 FD03 to allow for an additional number of *n* cutback steps prior to enabling the unstable propagation. Details are provided in the Abaqus User's Guide [11].
- Further improvements to the Abaqus/Standard finite element code were made recently and a *position=nonlocal* parameter was added to smooth out the tangential direction of individual crack segments along the crack front using a least squares procedure [11]. These improvements were made to smooth out jagged fronts which were observed previously during automated delamination propagation under predominantly mode II mixed-mode conditions (e.g. $G_{II}/G_T \geq 0.8$) [13][20].

An overview of recent Abaqus/Standard improvements is provided in Table A1 in the appendix which also highlights the associated new syntax. More detailed input syntax for the different analysis options in Abaqus/Standard is discussed in Table A2 and a list of all analyses performed with relevant input parameters is provided in Table A3 in the appendix.

ASSESSMENT OF RESULTS FROM AUTOMATED PROPAGATION ANALYSES

In the present section, the delamination prediction capabilities implemented in Abaqus/Standard 2021 FD06 are assessed using the C-ELS benchmark case developed above. For the general assessment, the 2D and 3D FE models shown in Figures 2 and 3 were used. Additionally, the effect of a misaligned mesh on automated crack propagation results was investigated using the 3D models shown in Figure 4.

The propagation analysis in Abaqus/Standard was performed in two steps starting from two initial delamination lengths, a_0=50.0 mm and 75.0 mm. In the first step, a tip deflection of about 90% w_c (w=6.0 mm) was applied to the model so that the region of linear load/displacement behavior could be analyzed quickly. During this first step, large displacement increments were allowed and automated propagation was disabled. In the second step, the center deflection was increased from w=6.0 mm to w=15.0 mm. Automated propagation was enabled and the B-K criterion for mixed-mode failure was selected. The following input parameters were kept constant for all analyses:

- The release tolerance was set to *reltol*=0.01.
- The limit for the smallest increment size was set equal to 10^{-20} to reduce the risk of numerical instability and early termination of the analysis and allow for sufficient cutback during the propagation phase of the analysis.
- The number of total increments was limited to 5000.
- For contact stabilization, the stabilization factor was set to 10^{-6}.

Results from 2D analyses

Example results using Abaqus/Standard are shown in Figures 14 and 15 where the computed resulting load (load P) at the tip of the C-ELS specimen (Figures 1 and 2) is plotted versus the applied tip deflection (w) for different parameter settings in Abaqus/Standard. For a_0=50.0 mm, the initial load drop occurred near the critical point (P_c and w_c) for all settings studied and the delamination propagation started (colored dashed lines), as shown in Figure 14. After reaching the peak, the load continued to drop during unstable propagation without any increase in applied displacement. The computed load/displacement path converged to the stable propagation branch of the benchmark result (solid grey line). Differences, however, were observed in computational effort. The *step* option, which invokes immediate node release, required 201 analysis increments. The *ramp* option, which allows for a gradual release, required 588 analysis increments. For the combined *ramp* and *unstable growth tolerance* options, the unstable propagation (vertical drop in load) occurred at slightly higher displacements compared to the benchmark when the default settings (*unstable growth tolerance*=∞*; n*=0*)* were used (dark blue dashed line). For this option, 262 analysis increments were required. Results closer to the benchmark (light blue dashed line) were obtained when the scaling parameter n was explicitly defined (n=1) which allowed for an additional cutback prior to enabling the unstable propagation in Abaqus/Standard; however, this increased the required analysis increments to 268 [11]. A drop in load is observed for w=10 mm after which the delamination starts propagating into the clamped zone of the mesh.

The results obtained for an initial delamination length, a_0=75.0 mm, are shown in Figure 15 (colored dashed lines). Although there isn't any unstable propagation phase in this case, the same input parameters as in the above example were used for consistency and to explore any potential negative effects on the analysis. All computed load/displacement paths (colored lines) followed the stable propagation branch of the benchmark result (solid grey line). Again, a drop in load is observed for w=10 mm after which the delamination starts propagating into the clamped zone of the mesh.

Results from 3D analyses

Example results obtained from 3D analyses are presented in the following section for starter delamination lengths a_0=50 mm and a_0=75 mm. Models with aligned (straight) and misaligned (angled) meshes were used, as shown in Figures 3 and 4, respectively. Two mesh sizes were studied with a baseline mesh where the element lengths at the delamination tip and the section of automated crack propagation was Δa=0.5 mm and the element size across the width was ΔB=1.0 mm. A second 3D model with a refined mesh across the width with ΔB=0.5 mm element size was used for additional refinement studies. The load/displacement results computed during the automated propagation analysis were compared to the benchmark solution established earlier. The computed delamination front contours in the plane of delamination were used as an additional qualitative measure.

Results for an initial delamination length a_0=50 mm

Computed load/displacement results obtained from models with aligned mesh

Example results using the aligned (straight) mesh are shown in Figures 16 through 19 where the computed resulting load (P) at the tip of the C-ELS specimen (Figures 1 and 2) is plotted versus the applied tip deflection (w) for different parameter settings in Abaqus/Standard. For the original Abaqus/Standard input parameters *step* and *ramp,* the results are shown in Figure 16. For the *step* option (solid red curve), which invokes immediate node release, the initial load drop occurred prior to the critical point (P_c and w_c). Subsequently, the unstable propagation (vertical drop in load) ran parallel to the benchmark solution. Past the unstable path, the results qualitatively followed the trend seen in the benchmark solution, however, never converged to the critical path (open grey circles and solid grey line). For the *ramp* option (solid green line) a small initial load drop occurred near the critical point (P_c and w_c). After some additional load increase, the unstable propagation occurred for a slightly higher applied displacement compared to the benchmark. Following the vertical drop in load, the computed results converged to the benchmark solution.

For the *unstable growth tolerance* option, the analysis terminated immediately following the first load drop when the default settings (*unstable growth tolerance*=∞*; n*=0) were used as shown in Figure 17 (solid blue line). Results closer to the benchmark (solid green line) were obtained when the scaling parameter n was explicitly defined (n=1) and the *position=nonlocal* parameter was added to smooth out the tangential direction of individual crack segments along the crack front during the analysis. An overshoot was observed (solid red line) when the scaling parameter n was increased (n=2) which allowed for two additional cutbacks prior to enabling the unstable propagation algorithm. Mostly, the results oscillated around the critical path.

For additional comparison, the parameter α was changed in one set of analyses to the default value (α=0.5) for which the results are shown in Figure 18. The *position=nonlocal* parameter was used for all analyses. The default settings (*unstable growth tolerance*=∞*; n*=0) yielded the best results (solid green line) with regard to capturing the vertical load drop. When the scaling parameter n was explicitly defined (n=1) the vertical drop occurred prior to the critical point. For n=2 an overshoot was observed as before when using this value. Largely, all results oscillated around the critical path as observed before, so that guidance for using a particular value of α cannot be made at this point.

Further studies were performed using a refined mesh (ΔB=0.5 mm) in the width direction. The results are shown in Figure 19 for all parameters varied. For the *step* option (thick solid purple curve), the analysis terminated immediately following the first load drop near the critical point. For the *ramp* option (thick solid light blue line), the initial load drop occurred near to the critical point followed by the load drop associated with unstable delamination propagation. The analysis closely tracks the stable part of the benchmark case and then terminates because smaller increments are required than the limit (10^{-20}) specified. For the *unstable growth tolerance* options investigated

- *unstable growth tolerance*=∞*; n*=1 (solid dark blue line)
- *unstable growth tolerance*=∞*; nonlocal, n*=1 (solid green line)
- *unstable growth tolerance*=∞*; nonlocal, n*=2 (solid red line)

the analyses completed without numerical issues. Only the analysis for *n*=2 terminated early due to a defined maximum that limits the total number of increments for an analysis. In general, the results adequately track the benchmark case. The oscillations observed are less pronounced when compared to the results for ΔB=1.0 mm shown in Figure 18, which is attributed to the refined mesh used.

Computed load/displacement results obtained from models with misaligned mesh

Example results using the misaligned (angled) mesh are shown in Figures 20 through 22. For the original Abaqus/Standard input parameters *step* and *ramp* the results are shown in Figure 20. For the *step* option (solid red curve) the initial load drop occurred prior to the critical point (P_c and w_c). Subsequently, the unstable propagation (vertical drop in load) was offset in comparison to the benchmark solution. Past the unstable path, the results qualitatively followed the trend seen in the benchmark solution, however, only converged to the critical path (open grey circles and solid grey line) for w>9.5 mm when the delamination approached the clamped region of the specimen. For the *ramp* option (solid green line), the analysis terminated immediately following the first load drop near the critical point.

For the *unstable growth tolerance* option, the first load drop occurred prior to the critical point when the default settings (*unstable growth tolerance*=∞*; n*=0) were used as shown in Figure 21 (solid blue line). Results close to the benchmark (solid green line) were obtained when the scaling parameter *n* was explicitly defined (*n*=1) and the *position=nonlocal* parameter was added. Similar results were observed when the scaling parameter *n* was increased (*n*=2) which allowed for two additional cutbacks prior to enabling the unstable propagation algorithm (solid red line). Mostly, the results obtained for the settings that include the *unstable growth tolerance* option oscillated around the critical solution.

Additional studies were performed using a refined mesh (ΔB=0.5 mm) in width direction. The results are shown in Figure 22 for all parameters varied. For the *step* option (thick solid purple curve) and *ramp* option (thick solid light blue line), the analysis terminated immediately following the first load drop prior to reaching the critical point. For the *unstable growth tolerance* options investigated

- *unstable growth tolerance*=∞*; n*=1 (solid dark blue line)
- *unstable growth tolerance*=∞*; nonlocal, n*=1 (solid green line)
- *unstable growth tolerance*=∞*; nonlocal, n*=2 (solid red line)

the analyses completed without numerical issues and results closely track the stable part of the benchmark case. Only the analysis for *n*=2 terminated early due to a defined maximum that limits the total number of increments for an analysis. In general, the oscillations observed are less pronounced when compared to the results for ΔB=1.0 mm shown in Figure 21, which is attributed to the refined mesh used.

The results obtained from aligned and misaligned meshes for unstable delamination propagation (a_0=50 mm) suggest that the step option should not be used in order to avoid inaccurate results. Rather, progressive nodal release using the ramp option should be used during automated propagation. These results appeared to be the most accurate when compared to the benchmark; however, they often suffered from early terminations because smaller increments were required than the limit (10^{-20}) specified, or the number of total increments allowed (5000) was too small. In general, improved convergence was obtained in fewer increments when the *unstable growth tolerance* option in combination with the *position=nonlocal* option were added to the analysis. The most reliable results were obtained for a scaling parameter *n*=1. Smoother results, with less deviation from the benchmark were obtained with a refined mesh in width direction (ΔB=0.5 mm).

Computed delamination front contours

Computed delamination front contours obtained from analyses using aligned and misaligned meshes are shown in Figures 23 and 24, respectively, which provide a top view of the plane of delamination. To visualize the delamination condition, the state variable *bdstat* in Abaqus/Standard was plotted. The initial condition with a straight delamination front is shown in Figure 23(a) where the delaminated section is shown as the blue surface and the intact section is shown as the red surface. The green/yellow zone represents the location of the delamination front. Growth contours obtained from the mesh with ΔB=1.0 mm are shown for the different input settings in Figures 23(b) through (f). The columns represent three stages during propagation: onset, propagation during the analyses, and the final front. One example obtained from the refined mesh (ΔB=0.5 mm) is shown in Figure 23(g). For all parameters studied, the delamination starts to grow slightly first at the two edges due to the distribution of the energy release which spikes near the edges as discussed earlier (see Figure 10). During propagation, the front remains relatively straight across the width. Locally, however, zig-zag approximation of the front is observed where certain elements release sooner than neighboring elements. This appears to be an artifact of the VCCT implementation in Abaqus/Standard. In extreme cases this can lead to elements that never fully release when all the surrounding elements have already completely released. In the contour plot this is seen as local *green islands* in the delaminated blue section (see center and right columns in Figure 23(d) to (g)). This artifact was supposed to have been removed with the introduction of the *position=nonlocal* parameter which was added to smooth out the tangential direction of individual crack segments along the crack front using a least squares procedure. Additional adjustments to the VCCT implementation in Abaqus/Standard may be required. The roughness of the front approximation is somewhat alleviated by choosing a finer mesh across the width as shown in Figure 23(g). The formation of *islands*, however, remains an issue.

Front contours obtained from the analyses using a misaligned (angled) mesh are shown in Figure 24. Note that the initial condition with a straight delamination front can only be approximated due to the nature of the mesh as shown in Figure 24(a). Locally artificial *corners* appear which are an artifact of representing a straight front with the misaligned mesh. As before, growth contours obtained from the mesh with ΔB=1.0 mm are shown for the different input settings in Figures 24(b) through (f). One example obtained from the refined mesh (ΔB=0.5 mm) is shown in Figure 24(g). As in Fig. 23, the delamination starts to grow slightly first at the two edges due to the distribution of the energy release which spikes near the edges, as discussed earlier (see Figure 10). Additionally, growth occurs locally at the *corners* mentioned above where the energy release rate is somewhat higher (see left column in Figures 24(b) to (f)). For the *step* option (Figure 24(b)), a slanted front developed and propagated in a self-similar manner until the end of the analysis. For the *ramp* option (Figure 24(c)), the analysis terminated soon after propagation started. For the *unstable growth tolerance* options investigated

- *unstable growth tolerance*=∞*; n*=1 (Figure 24(d))
- *unstable growth tolerance*=∞*; nonlocal, n*=1 (Figure 24(e))
- *unstable growth tolerance*=∞*; nonlocal, n*=2 (Figure 24(f))

a relatively straight front across the width developed during propagation. Locally, however, zig-zag approximation of the front is observed, as discussed above, where certain elements release sooner than neighboring elements. A case where several elements along the front are in the process of releasing simultaneously is shown in Figure 24 (f) (see green zone in center figure). As before, the roughness of the front approximation is somewhat alleviated by choosing a finer mesh across the width as shown in Figure 24(g).

Results for an initial delamination length a_0=75 mm

The key motivation to pursue the C-ELS benchmark compared to the ENF was that stable delamination propagation can be obtained for a larger region of the specimen. This enables study of how the observations made in the previous section change when simulating stable delamination growth. For example, is the zig-zag front observed locally for unstable growth (see Figures 23 and 24) caused by an increase in energy release rate with delamination length (positive dG/da)? One explanation is that after node release the new node at the locally advanced front experiences a higher energy release rate. Therefore, these new nodes would now be eligible to release rather than the neighboring nodes, causing the observed continued roughness across the width or in extreme cases the development of *islands* mentioned above. To investigate this hypothesis, an additional set of analyses were performed with an initial starter delamination length a_0=75 mm for which stable delamination growth is expected.

Computed load/displacement results obtained from models with aligned mesh

Example results using the aligned (straight) mesh are shown in Figures 25 through 27 where the computed resulting load (load *P*) at the tip of the C-ELS specimen (Figures 1 and 2) is plotted versus the applied tip deflection (*w*) for different parameter settings in Abaqus/Standard. For the original Abaqus/Standard input parameters *step* and *ramp* the results are shown in Figure 25. For the *step* option (solid red curve), which invokes immediate node release, the initial load drop occurred prior to reaching the critical solution (open grey circles and solid grey line). Subsequently, an unstable propagation (vertical drop in load) occurred followed by stable results which qualitatively followed the trend seen in the benchmark solution. Results, however, only converged to the critical solution for w>9.5 mm when the delamination approached the clamped region of the specimen. For the *ramp* option (solid green line), which allows for a gradual release, a small initial load drop occurred near the critical solution. After some additional load increase, the computed results tracked the benchmark solution.

For the *unstable growth tolerance* option used, result are plotted in Figure 26. For all cases studied, a small initial load drop occurred near the critical solution. After some additional load increase, all computed results oscillated around the benchmark solution. Typically, the result for *unstable growth tolerance* and *n*=1 stayed below the benchmark result (solid blue line). Small changes were observed when the *position=nonlocal* parameter was added to smooth out the tangential direction of individual crack segments along the crack front during the analysis (solid green line). An overshoot was observed (solid red line) when the scaling parameter *n* was increased (*n*=2) which allowed for two additional cutbacks prior to enabling the unstable propagation algorithm.

Further studies were performed using a refined mesh (ΔB=0.5 mm) in the width direction. The results are shown in Figure 27 for all parameters varied. For the *step* option (solid purple curve), the initial load drop occurred prior to reaching the critical solution (open grey circles and solid grey line). Subsequently, an unstable propagation (vertical drop in load) occurred, followed by stable results which qualitatively followed the trend seen in the benchmark solution. The analysis then terminated because smaller increments were required than the limit (10^{-20}) specified. For the *ramp* option (thick light blue line), the initial load drop occurred near the critical solution followed by an immediate analysis termination due to the same numerical issue. For the *unstable growth tolerance* options investigated

- *unstable growth tolerance=∞; n*=1 (solid dark blue line)
- *unstable growth tolerance=∞; nonlocal, n*=1 (solid green line)
- *unstable growth tolerance=∞; nonlocal, n*=2 (solid red line)

the analyses completed without numerical issues. In general, the results adequately tracked the benchmark case. The oscillations observed are less pronounced when compared to the results for ΔB=1.0 mm shown in Figure 26 which is attributed to the refined mesh used.

Computed load/displacement results obtained from models with misaligned mesh

Example results using the misaligned (angled) mesh are shown in Figures 28 through 30. For the original Abaqus/Standard input parameters *step* and *ramp,* the results are shown in Figure 28. For the *step* option (solid red curve) the initial load drop occurred prior to reaching the critical solution w_c (open grey circles and solid grey line). Subsequently, an unstable propagation (vertical drop in load) was observed. Past the unstable path, the results qualitatively followed the trend seen in the benchmark solution, however, only converged to the critical path for w>9.5 mm when the delamination approached the clamped region of the specimen. For the *ramp* option (solid green line), the analysis terminated immediately following the first load drop near the critical solution.

For the *unstable growth tolerance* option, the first load drop occurred prior to reaching the critical solution when *unstable growth tolerance*=∞ was used in combination with *n*=1 as shown in Figure 29 (solid blue line). Results close to the benchmark (solid green line) were obtained when the *position=nonlocal* parameter was added. Similar results were observed when the scaling parameter *n* was increased (*n*=2) which allowed for two additional cutbacks prior to enabling the unstable propagation algorithm (solid red line). Mostly, the results obtained for the settings that include the *unstable growth tolerance* option oscillated around the critical solution.

Additional studies were performed using a refined mesh (ΔB=0.5 mm) in the width direction. The results are shown in Figure 30 for all parameters varied. For the *step* option (solid purple curve) the initial load drop occurred prior to reaching the critical solution (open grey circles and solid grey line). Subsequently, the analysis qualitatively followed the trend seen in the benchmark solution and then terminated because smaller increments were required than the limit (10^{-20}) specified. For the *ramp* option (thick light blue line), the analysis terminated immediately following the first load drop prior to reaching the critical solution. For the *unstable growth tolerance* options investigated

- *unstable growth tolerance*=∞*; n*=1 (solid dark blue line)
- *unstable growth tolerance*=∞*; nonlocal, n*=1 (solid green line)
- *unstable growth tolerance*=∞*; nonlocal, n*=2 (solid red line)

the analyses completed without numerical issues and results closely tracked the stable part of the benchmark case. Only the analysis for *n*=2 terminated early due to a defined maximum that limits the total number of increments for an analysis. In general, the oscillations observed are less pronounced when compared to the results for ΔB=1.0 mm shown in Figure 29, which is attributed to the refined mesh used.

The results obtained from aligned and misaligned meshes for stable delamination propagation (a_0=75 mm) confirm that the step option should not be used in order to avoid inaccurate results. Rather, progressive nodal release using the ramp option should be used during automated propagation. These results appeared to be the most accurate when compared to the benchmark, however, often suffered from early terminations because smaller increments were required than the limit (10^{-20}) specified or the number of total increments allowed (5000) was too small. In general, improved convergence was obtained in fewer increments when the *unstable growth tolerance* option in combination with the *position=nonlocal* option was added to the analysis. The most reliable results were obtained for a scaling parameter *n*=1. Smoother results with less deviation from the benchmark were obtained with a refined mesh in width direction (ΔB=0.5 mm).

Computed delamination front contours

Computed delamination front contours obtained from analyses using aligned and misaligned meshes are shown in Figures 31 and 32, respectively. To visualize the delamination condition, the state variable *bdstat* in Abaqus/Standard was plotted. The initial condition with a straight delamination front is shown in Figure 31(a) for the aligned mesh. Growth contours obtained from the mesh with ΔB=1.0 mm are shown for the different input settings in Figures 31(b)

through (f). As with the models with a_0=50 mm, for all parameters studied, the delamination starts to grow slightly first at the two edges. One example obtained from the refined mesh (ΔB=0.5 mm) is shown in Figure 31(g). During propagation, the front remains relatively straight across the width. Locally, however, zig-zag approximation of the front is again observed. Local *green islands* can be seen in the delaminated blue section in Figure 31(d) to (g)). The roughness of the front approximation is somewhat alleviated by choosing a finer mesh across the width as shown in Figure 31(g). The formation of *islands*, however, remains an issue.

Front contours obtained from the analyses using a misaligned (angled) mesh are shown in Figure 32. Note that the initial condition with a straight delamination front can only be approximated due to the nature of the mesh as shown in Figure 32(a). Locally artificial *corners* appear which are an artifact of representing a straight front with the misaligned mesh. As before, growth contours obtained from the mesh with ΔB=1.0 mm are shown for the different input settings in Figures 32(b) through (f). One example obtained from the refined mesh (ΔB=0.5 mm) is shown in Figure 32(g). As in all the previous cases, for all parameters studied, the delamination starts to grow slightly first at the two edges. Additionally, growth occurs locally at the *corners* mentioned above where the energy release rate is somewhat higher (see left column in Figures 32(b) to (f)). For the *step* option (see Figure 32(b)), a somewhat slanted front developed and propagated in a nearly self-similar manner until the end of the analysis. For the *ramp* option (Figure 32(c)), the analysis terminated soon after propagation started. For the *unstable growth tolerance* options investigated

- *unstable growth tolerance*=∞*; n*=1 (Figure 32(d))
- *unstable growth tolerance*=∞*; nonlocal, n*=1 (Figure 32(e))
- *unstable growth tolerance*=∞*; nonlocal, n*=2 (Figure 32(f))

a relatively straight front across the width developed over the course of automated delamination propagation. Locally, however, zig-zag approximation of the front is observed, as discussed above, where certain elements release sooner than neighboring elements. In the contour plot this is seen as local *green islands* in the wake of the front in the delaminated blue section (see center and right columns in Figure 32(d) and(e). Additional adjustments to the VCCT implementation in Abaqus/Standard may be required. The roughness of the front approximation is somewhat alleviated by choosing a finer mesh across the width as shown in Figure 32(g).

The results obtained from both aligned and misaligned meshes suggest that an increase in energy release with delamination length (positive *dG*/*da*) is not the cause for the development of zig-zagged fronts or unreleased elements (islands) in the wake of the delamination front as hypothesized. These zig-zagged fronts also developed from a starter front at a_0=75 mm for which delamination propagation is stable. Increment numbers shown in the right most column indicate that the ramp option requires many analysis increments for the delamination to reach the clamped region of the specimen. Significantly fewer increments are required when the unstable growth tolerance option is added. However, this advantage is reduced as the scaling parameter *n* is increased. These observations confirm earlier results obtained from 2D analyses.

SUMMARY AND CONCLUSIONS

The development of a benchmark example based on Linear Elastic Fracture Mechanics (LEFM) and VCCT was shown in detail for the Calibrated End-Loaded Split (C-ELS) specimen. The benchmarking procedure is independent of the analysis software and can be used to assess the performance of automated delamination prediction capabilities in finite element codes.

First, the development of a new VCCT-based benchmark case for crack propagation prediction under quasi-static loading was discussed in detail. Second, the application was demonstrated for the commercial finite element code Abaqus/Standard 2021 FD06. Third,

results obtained from VCCT-based, automated quasi-static propagation analysis were compared to the benchmark cases. The results showed the following:

- In general, good agreement between the results obtained from the quasi-static propagation analysis and the benchmark results could be achieved by selecting the appropriate input parameters.
- For Abaqus/Standard 2021 FD06 in particular, the results for automated delamination propagation analysis under quasi-static loading showed the following:
    - Good agreement between analysis results and the benchmarks could be achieved for release tolerance values (*reltol*=0.01) in combination with contact stabilization (cs=1x10^{-6}). These results confirmed previous observations.
    - The use of the step option is not recommended in order to avoid inaccurate results.
    - Progressive nodal release using the ramp option should be used during automated propagation. These results appeared to be the most accurate when compared to the benchmark, however, required many increments and often suffered from numerical problems which led to premature analysis termination since smaller increments were required than the limit (10^{-20}) specified.
    - Improved convergence can be obtained in fewer increments when the *unstable growth tolerance* option in combination with the *position=nonlocal* option is added to the analysis.
    - The load/displacement results in the propagation phase of the analysis results appeared smoother with less pronounced oscillations when a refined mesh was used not only in the delamination propagation (Δa=0.5 mm) but also in the width direction (ΔB=0.5 mm).
    - The C-ELS benchmark with stable and unstable regions of delamination propagation was useful in investigating the hypothesis that the zig-zag front observed locally for unstable growth is caused by an increase in energy release rate with delamination length (positive dG/da). However, delamination front contours showed a zig-zag behavior with unreleased elements developing (islands) in the wake of the front regardless of the delamination propagation being stable or unstable. Thus, the hypothesis could not be confirmed. The source may be in the VCCT-implementation which needs to be further investigated.

Overall, the benchmark case enabled study of solution parameters that give the most reliable solution with regards to accuracy and convergence. Further, the ability to assess the continuous improvements in one finite element code illustrates the value of establishing benchmark solutions. In the context of analysis *Verification and Validation* (V&V), these benchmarks may also be used for code and calculation verification purposes and thus serve as a valuable tool for software developers. Specifically, these benchmark results may be used to evaluate other algorithms for delamination prediction, such as cohesive elements and adaptive mesh VCCT algorithms.

Additional analyses are required to study the observed zig-zag fronts and areas with unreleased elements (islands) in the wake of the front. Subsequently, studies are required to validate the analyses against experimental results obtained from these and other simple characterization specimens. Further, a thorough comparison of analysis and test results of real world problems on the coupon, element and sub-component levels are required before the numerical approach can be used confidently to predict delamination propagation.

ACKNOWLEDGEMENTS

This research was supported by the Revolutionary Vertical Lift Technology Project (RVLT) as part of NASA's Advanced Air Mobility Mission within the Aeronautics Research Mission Directorate (ARMD).

The authors would like to thank Zhen-zhong Du, SIMULIA R&D Technology Director, for the valuable input and support he provided to the authors performing these analyses.

REFERENCES

[1] T. E. Tay, "Characterization and analysis of delamination fracture in composites - An overview of developments from 1990 to 2001," *Appl. Mech. Rev.*, vol. 56, no. 1, 2003, pp. 1–32.

[2] I. S. Raju and T. K. O'Brien, "Fracture mechanics concepts, stress fields, strain energy release rates, delamination and growth criteria," in *Delamination behaviour of composites*, Srinivasan Sridharan, Ed. Woodhead Publishing in Materials, 2008.

[3] E. F. Rybicki and M. F. Kanninen, "A Finite Element Calculation of Stress Intensity Factors by a Modified Crack Closure Integral," *Eng Fract. Mech*, vol. 9, 1977, pp. 931–938.

[4] Ronald Krueger, "The Virtual Crack Closure Technique for Modelling Interlaminar Failure and Delamination in Advanced Composite Materials," in *Numerical Modelling of Failure in Advanced Composite Materials*, Pedro Camanho and Stephen Hallett, Eds. Woodhead Publishing Ltd, 2015, pp. 3–53.

[5] "Guide for Verification and Validation in Computational Solid Mechanics," The American Society of Mechanical Engineers, ASME V&V 10-2006, 2006.

[6] Ronald Krueger, "A summary of benchmark examples and their application to assess the performance of quasi-static delamination propagation prediction capabilities in finite element codes," *J. Compos. Mater.*, vol. 49, no. 26, 2015, pp. 3297–3316.

[7] Ronald Krueger, Lyle Deobald, and Haozhong Gu, "A Benchmark Example for Delamination Propagation Predictions Based on the Single Leg Bending Specimen under Quasi-static and Fatigue Loading," presented at the ASC 33rd Technical Conference, 2018.

[8] Ronald Krueger, Lyle Deobald, and Haozhong Gu, "A Benchmark Example for Delamination Growth Predictions Based on the Single Leg Bending Specimen under Fatigue Loading," *Adv. Model. Simul. Eng. Sci.*, vol. 7, no. 11, 2020.

[9] Adrian C. Orifici and Ronald Krueger, "Assessment of Static Delamination Propagation Capabilities in Commercial Finite Element Codes Using Benchmark Analysis," NASA/CR-2010-216709, NIA report no. 2010-03, 2010.

[10] Ronald Krueger, "Application of Benchmark Examples to Assess the Single and Mixed-Mode Static Delamination Propagation Capabilities in ANSYS," NASA/CR-2012-217588, NIA report no. 2012-04, 2012.

[11] "Abaqus Analysis User's Guide - Abaqus 2021," DS Simulia Corp., Providence, RI, USA., 2021.

[12] "D7905/D7905M-14 Standard Test Method for Determination of the Mode II Interlaminar Fracture Toughness of Unidirectional Fiber-Reinforced Polymer Matrix Composites," in *Annual Book of ASTM Standards*, vol. 15.03, ASTM International, 2014.

[13] Ronald Krueger, "Development and Application of Benchmark Examples for Mode II Static Delamination Propagation and Fatigue Growth Predictions," NASA/CR-2011-217305, NIA report no. 2011-02, 2011.

[14] B. R. K. Blackman, A. J. Brunner, and J. G. Williams, "Mode II fracture testing of composites: a new look at an old problem," *Eng. Fract. Mech.*, vol. 73, no. 16, Nov. 2006, pp. 2443–2455.

[15] J. Bertrand, J. Jumel, J. Renart, and J.-B. Kopp, "Theoretical assessment of ELS test data reduction technique using virtual testing," *Int. J. Fract.*, vol. 229, no. 2, Jun. 2021, pp. 195–213.

[16] "ISO 15114:2014 Fibre-reinforced plastic composites -- Determination of the mode II fracture resistance for unidirectionally reinforced materials using the calibrated end-loaded split (C-ELS) test and an effective crack length approach," ISO (International Organization for Standardization)., 2014.

[17] M. L. Benzeggagh and M. Kenane, "Measurement of mixed-mode delamination fracture toughness of unidirectional glass/epoxy composites with mixed-mode bending apparatus," *Compos. Sci. Technol.*, vol. 56, no. 4, 1996, pp. 439–449.

[18] Gerald E. Mabson, Nelson V. De Carvalho, and Ronald Krueger, "VCCT with Progressive Nodal Release for Simulating Mixed-Mode Delamination: Formulation, Algorithmic Improvements," presented at the ASC 33rd Technical Conference, 2018.

[19] Lyle R. Deobald *et al.*, “Guidelines for VCCT-based Interlaminar Fatigue and Progressive Failure Finite Element Analysis,” NASA/TM–2017-219663, 2017.
[20] Ronald Krueger, “Development and Application of Benchmark Examples for Mixed-Mode I/II Quasi-Static Delamination Propagation Predictions,” NASA/CR-2012-217562, NIA report no. 2012-01, 2012.
[21] T. Kevin O’Brien, William M. Johnston, and Gregory Toland, “Mode II Interlaminar Fracture Toughness and Fatigue Characterization of a Graphite Epoxy Composite Material,” NASA/TM-2010-216838, 2010.
[22] Gretchen B. Murri, “Evaluation of Delamination Onset and Growth Characterization Methods Under Mode I Fatigue Loading,” NASA/TM-2013-217966, 2013.
[23] James G. Ratcliffe and William M. Johnston Jr, “Influence of Mixed Mode I-Mode II Loading on Fatigue Delamination Growth Characteristics of a Graphite Epoxy Tape Laminate,” presented at the 29th ASC Technical Conference, 2014.

TABLES

Table I. Material Properties. [6]

Unidirectional Graphite/Epoxy Prepreg		
E_{11} = 161 GPa	E_{22} = 11.38 GPa	E_{33} = 11.38 GPa
ν_{12} = 0.32	ν_{13} = 0.32	ν_{23} = 0.45
G_{12} = 5.2 GPa	G_{13} = 5.2 GPa	G_{23} = 3.9 GPa

The material properties are given with reference to the ply coordinate axes where index 11 denotes the ply principal axis that coincides with the direction of maximum in-plane Young's modulus (fiber direction). Index 22 denotes the direction transverse to the fiber in the plane of the lamina and index 33 the direction perpendicular to the plane of the lamina.

Table II. Fracture Properties [21][22][23]

IM7/8552 Fracture Toughness Data		
G_{Ic} = 0.212 kJ/m^2	G_{IIc} =0.774 kJ/m^2	η= 2.1

APPENDIX

An overview of recent Abaqus/Standard improvements is provided in Table A1. Typical Abaqus/Standard input file syntax for automated propagation analysis is shown in Table A2. A list of all analyses performed with relevant input parameters is provided in Table A3.

Table A1: Summary of recent VCCT-specific modifications in ABAQUS.

Version	Progressive Quasi-Static Analysis	Abaqus Input Syntax
<2018 (Baseline)	• Multi-node pair 'STEP' release (no RAMP) • RAMP single node pair release • Contact stabilization and global damping • Original viscous damping introduced • Total G_{equiv} convergence tolerance • Elastic constraint stiffness the same for all three modes	***DEBOND,… DEBONDING FORCE=STEP** ***DEBOND,… DEBONDING FORCE=RAMP** *Referred to as original input*
2018 FD03	• RAMP multi-node pair release with UNSTABLE GROWTH TOLERANCE	***FRACTURE CRITERION,… unstable growth tol** ***CONTROLS, TYPE=NO CUTBACK SCALING** **α, β** *Referred to as new input*
2019 FD01	• Viscous damping algorithm improved • Mode dependent constraint stiffness during RAMP release introduced for static growth • Asymmetric Jacobian with and without unloading. Undocumented feature available only via environment file activation.	
2020 FD03	• New data entry for unstable growth tolerance to indicate how many cutbacks, n, allowed prior to the activation of the unstable growth tolerance in an increment	***FRACTURE CRITERION,… unstable growth tol** ***CONTROLS, TYPE=NO CUTBACK SCALING** **α, β, n**
2020FD04	• Release of bonded node begins only if at least one the neighboring partially opened nodes is fully released.	
2020FD05	• Internal crack front smoothing	***FRACTURE CRITERION,… unstable growth tol, position=nonlocal**
2021FD04	• Solver bug fixed which caused random analysis termination during VCCT based automated delamination propagation	
2021FD05	• Additional solver improvements	

Table A2. Input for automated VCCT-based delamination propagation

Typical input file for `DEBONDING FORCE=STEP` and `RAMP` option

```
…
*parameter
*** release tolerance tol=0.01
*** fracture toughness and BK exponent
 GIc   = 0.212
 GIIc  = 0.774
 GIIIc = 0.774
 eta=2.1
*STEP, INC= 1000
*** static analysis ***
*STEP, NLGEOM, INC= 5000
*STATIC
0.005, 1.0, 1.0E-20, 0.005
*CONTROLS,PARAMETERS=TIME INCREMENTATION
 ,,,,,,,50
*** fracture analysis using VCCT
*DEBOND,SECONDARY=VCCT_TOP,MAIN=VCCT_BOT,DEBONDING FORCE=RAMP, FREQ=1
*FRACTURE CRITERION,TYPE=VCCT,MIXED MODE BEHAVIOR=BK, TOLERANCE=<tol>
 <GIc>,<GIIc>,<GIIIc>,<eta>
*CONTACT CONTROLS, STABILIZE, MAIN=VCCT_BOT, SECONDARY=VCCT_TOP
 1.E-06, 0, 0.1
…
```

Typical input file for `unstable growth tolerance` option (default ∞)

```
…
*DEBOND,SLAVE=VCCT_TOP,MASTER=VCCT_BOT,DEBONDING FORCE=RAMP, FREQ=1
*FRACTURE CRITERION,TYPE=VCCT,MIXED MODE BEHAVIOR=BK, TOLERANCE=<tol>,
unstable growth tol
 <GIc>,<GIIc>,<GIIIc>,<eta>
** scaling parameters alpha=0.9, beta=1.E10 and n=1
*CONTROLS, TYPE=NO CUTBACK SCALING
0.9, 1.E10, 1
…
```

Typical input file for `unstable growth tolerance` option (default ∞) and `position=nonlocal`

```
…
*DEBOND,SLAVE=VCCT_TOP,MASTER=VCCT_BOT,DEBONDING FORCE=RAMP, FREQ=1
*FRACTURE CRITERION,TYPE=VCCT,MIXED MODE BEHAVIOR=BK, TOLERANCE=<tol>,
unstable growth tol, position=nonlocal
 <GIc>,<GIIc>,<GIIIc>,<eta>
** scaling parameters alpha=0.5, beta=1.E10 and n=1
*CONTROLS, TYPE=NO CUTBACK SCALING
0.5, 1.E10, 1
…
```

Table A3. Input parameters for release tolerance, unstable growth tolerance, and cutback scaling

File name	mesh	a_0 [mm]	ΔB [mm]	DF[†]	usgt[§]	pos[¶]	α[$]	β[$]	n[$]
2D_50_step	2D	50	1.0	step	-	-	-	-	-
2D_50_ramp	2D	50	1.0	ramp	-	-	-	-	-
2D_50_usgt	2D	50	1.0	ramp	✓	-	0.9	1E10	0
2D_50_usgt_n1	2D	50	1.0	ramp	✓	-	0.9	1E10	1
3D_50_step	aligned	50	1.0	step	-	-	-	-	-
3D_50_ramp	aligned	50	1.0	ramp	-	-	-	-	-
3D_50_usgt_n0	aligned	50	1.0	ramp	✓	-	0.9	1E10	0
3D_50_usgt_n1	aligned	50	1.0	ramp	✓	-	0.9	1E10	1
3D_50_ustg_n1_sm	aligned	50	1.0	ramp	✓	✓	0.9	1E10	1
3D_50_usgt_n2_sm	aligned	50	1.0	ramp	✓	✓	0.9	1E10	2
3D_50_usgt_a05_n0_sm	aligned	50	1.0	ramp	✓	✓	0.5	1E10	0
3D_50_usgt_a05_n1_sm	aligned	50	1.0	ramp	✓	✓	0.5	1E10	1
3D_50_usgt_a05_n2_sm	aligned	50	1.0	ramp	✓	✓	0.5	1E10	2
3D_50_w05_step	aligned	50	0.5	step	-	-	-	-	-
3D_50_w05_ramp	aligned	50	0.5	ramp	-	-	-	-	-
3D_50_w05_usgt	aligned	50	0.5	ramp	✓	-	0.9	1E10	1
3D_50_w05_usgt_sm	aligned	50	0.5	ramp	✓	✓	0.9	1E10	1
3D_50_w05_usgt_n2_sm	aligned	50	0.5	ramp	✓	✓	0.9	1E10	2
2D_75_step	2D	75	1.0	step	-	-	-	-	-
2D_75_ramp	2D	75	1.0	ramp	-	-	-	-	-
2D_75_usgt	2D	75	1.0	ramp	✓	-	0.9	1E10	0
2D_75_usgt_n1	2D	75	1.0	ramp	✓	-	0.9	1E10	1
3D_75_step	aligned	75	1.0	step	-	-	-	-	-
3D_75_ramp	aligned	75	1.0	ramp	-	-	-	-	-
3D_75_usgt_n1	aligned	75	1.0	ramp	✓	-	0.9	1E10	1
3D_75_usgt_n1_sm	aligned	75	1.0	ramp	✓	✓	0.9	1E10	1
3D_75_usgt_n2_sm	aligned	75	1.0	ramp	✓	✓	0.9	1E10	2
3D_75_w05_step	aligned	75	0.5	step	-	-	-	-	-
3D_75_w05_ramp	aligned	75	0.5	ramp	-	-	-	-	-
3D_75_w05_usgt	aligned	75	0.5	ramp	✓	-	0.9	1E10	1
3D_75_w05_usgt_sm	aligned	75	0.5	ramp	✓	✓	0.9	1E10	1
3D_75_w05_usgt_n2_sm	aligned	75	0.5	ramp	✓	✓	0.9	1E10	2
skew_x05_y10_step	skewed	50	1.0	step	-	-	-	-	-
skew_x05_y10_ramp	skewed	50	1.0	ramp	-	-	-	-	-
skew_x05_y10_usgt	skewed	50	1.0	ramp	✓	-	0.9	1E10	1
skew_x05_y10_usgt_sm	skewed	50	1.0	ramp	✓	✓	0.9	1E10	1
skew_x05_y10_usgt_n2_sm	skewed	50	1.0	ramp	✓	✓	0.9	1E10	2
skew_x05_y05_ramp	skewed	50	0.5	step	-	-	-	-	-
skew_x05_y05_step	skewed	50	0.5	ramp	-	-	-	-	-
skew_x05_y05_usgt	skewed	50	0.5	ramp	✓	-	0.9	1E10	1
skew_x05_y05_usgt_sm	skewed	50	0.5	ramp	✓	✓	0.9	1E10	1
skew_x05_y05_usgt_n2_sm	skewed	50	0.5	ramp	✓	✓	0.9	1E10	2
skew_a75_x05_y10_step	skewed	75	1.0	step	-	-	-	-	-
skew_a75_x05_y10_ramp	skewed	75	1.0	ramp	-	-	-	-	-
skew_a75_x05_y10_usgt	skewed	75	1.0	ramp	✓	-	0.9	1E10	1

skew_a75_x05_y10_usgt_sm	skewed	75	1.0	ramp	✓	✓	0.9	1E10	1
skew_a75_x05_y10_usgt_n2_sm	skewed	75	1.0	ramp	✓	✓	0.9	1E10	2
skew_a75_x05_y05_step	skewed	75	0.5	step	-	-	-	-	-
skew_a75_x05_y05_ramp	skewed	75	0.5	ramp	-	-	-	-	-
skew_a75_x05_y05_usgt	skewed	75	0.5	ramp	✓	-	0.9	1E10	1
skew_a75_x05_y05_usgt_sm	skewed	75	0.5	ramp	✓	✓	0.9	1E10	1
skew_a75_x05_y05_usgt_n2_sm	skewed	75	0.5	ramp	✓	✓	0.9	1E10	2

File names in **bold font** indicate results plotted and discussed in this report.

† `*DEBOND,SLAVE=VCCT_BOT,MASTER=VCCT_TOP,`**`DEBONDING FORCE=STEP`**`, FREQ=1`

§ `*FRACTURE CRITERION,TYPE=VCCT,MIXED MODE BEHAVIOR=BK, TOLERANCE=<tol>,`
`unstable growth tol`

¶ `*FRACTURE CRITERION,TYPE=VCCT,MIXED MODE BEHAVIOR=BK, TOLERANCE=<tol>,`
`unstable growth tol,` **`position=nonlocal`**

$ `*CONTROLS, TYPE=NO CUTBACK SCALING`
α, β, n

FIGURES

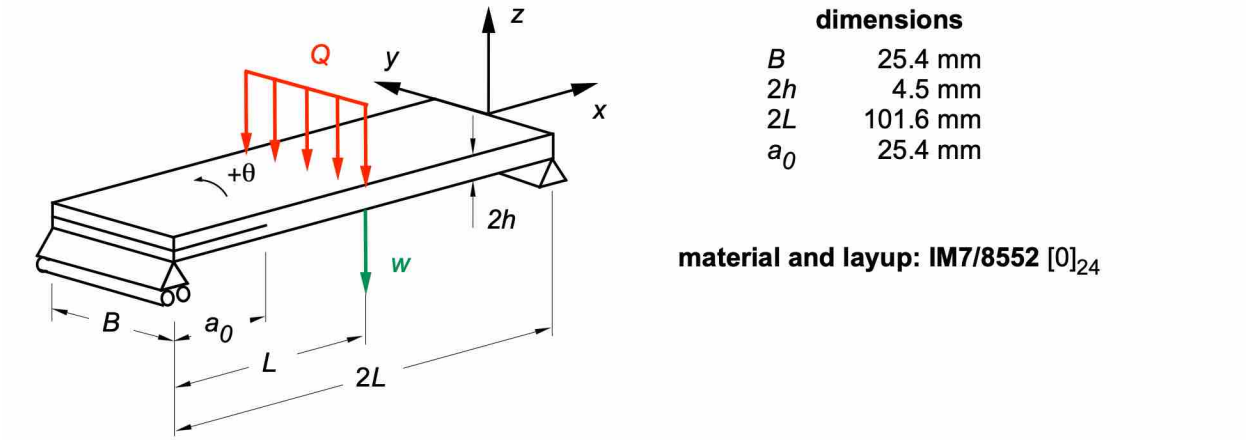

(a). *End-Notched Flexure Specimen (ENF).*

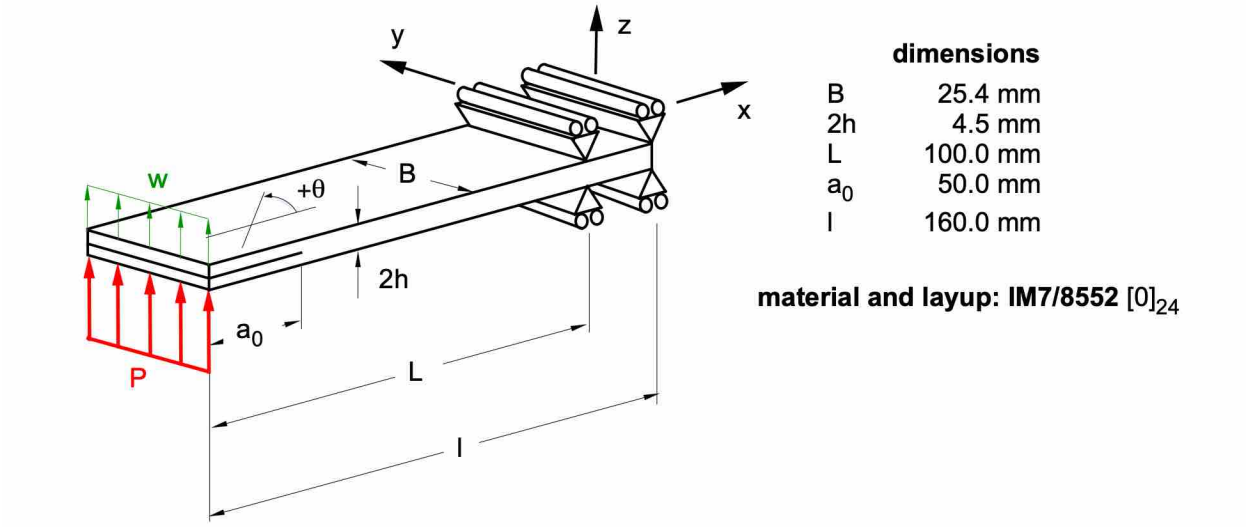

(b). *Calibrated End-Loaded Split Specimen (C-ELS).*

Figure 1. Standard test specimens for mode II fracture toughness characterization.

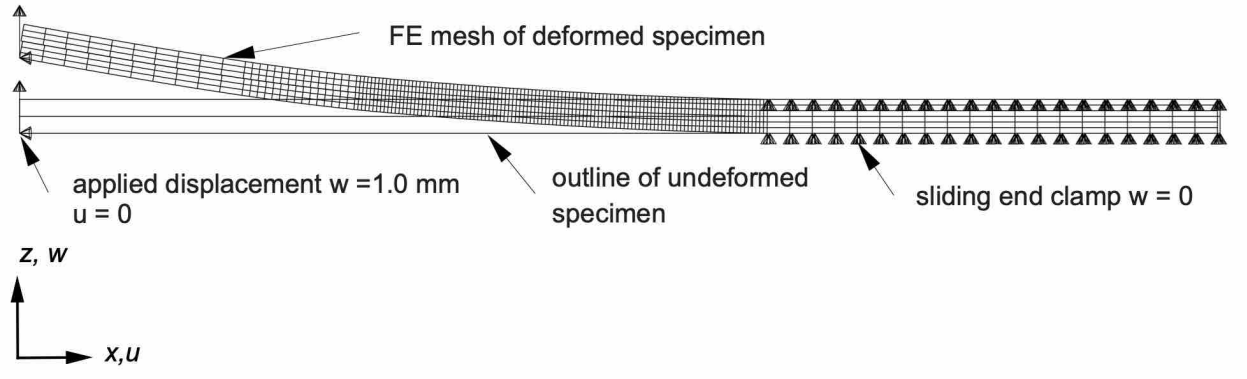

Figure 2. Two-dimensional (2D) finite element model of C-ELS specimen.

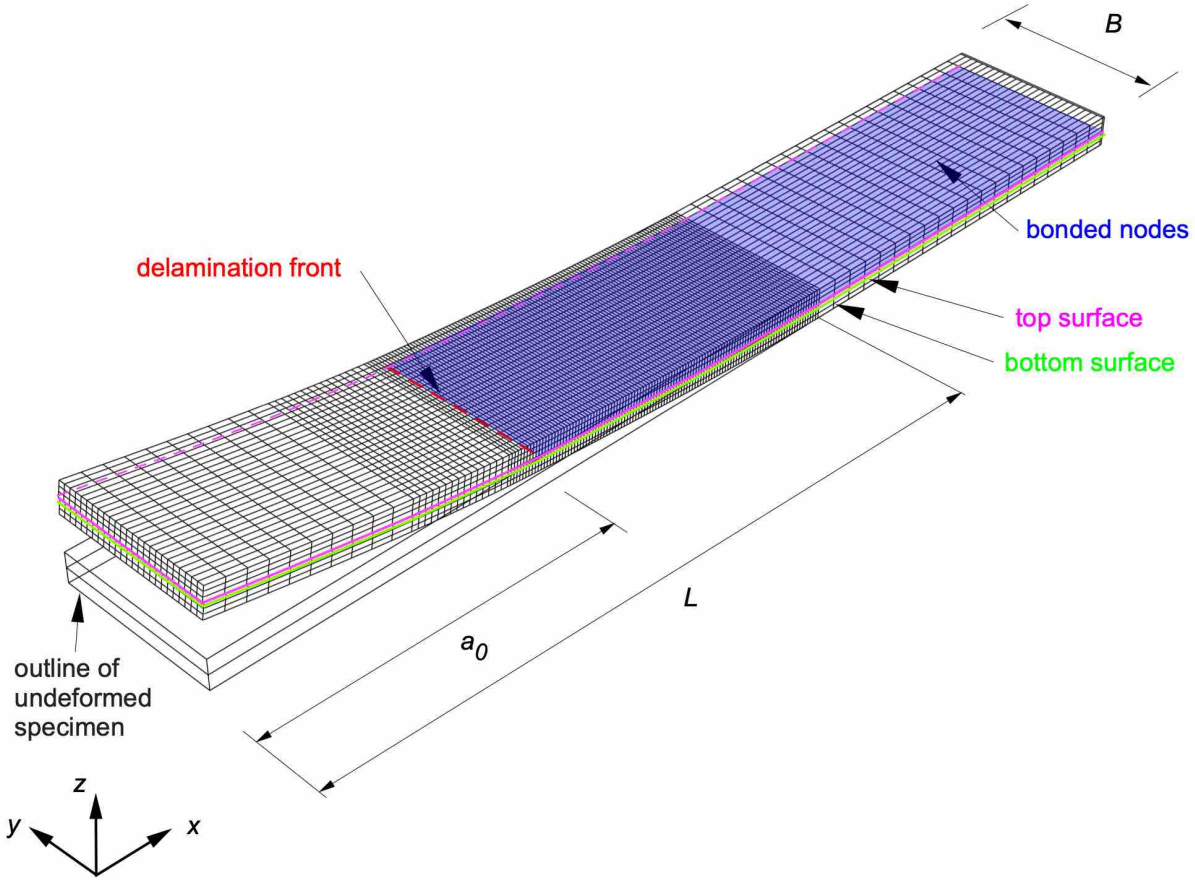

(a). *Mesh with element size Δa=0.5 mm in refined zone and ΔB=1.0 mm across the width.*

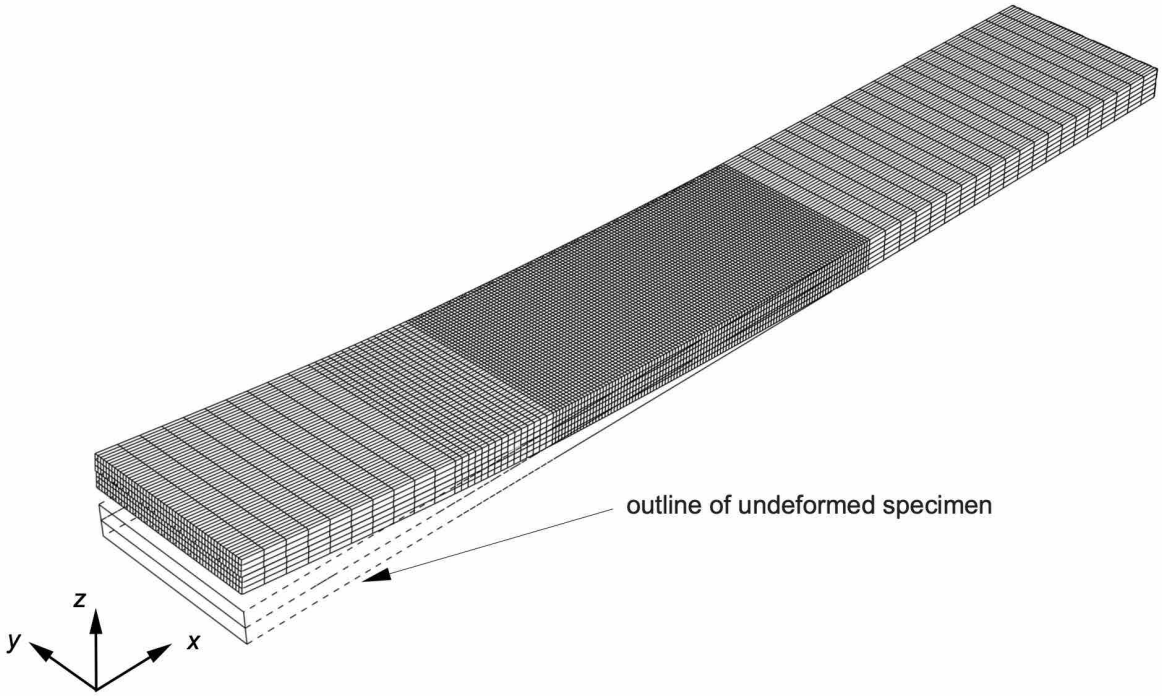

(b). *Mesh with element size Δa=0.5 mm in refined zone and ΔB=0.5 mm across the width.*

Figure 3. Three-dimensional (3D) FE models of C-ELS specimen with aligned mesh.

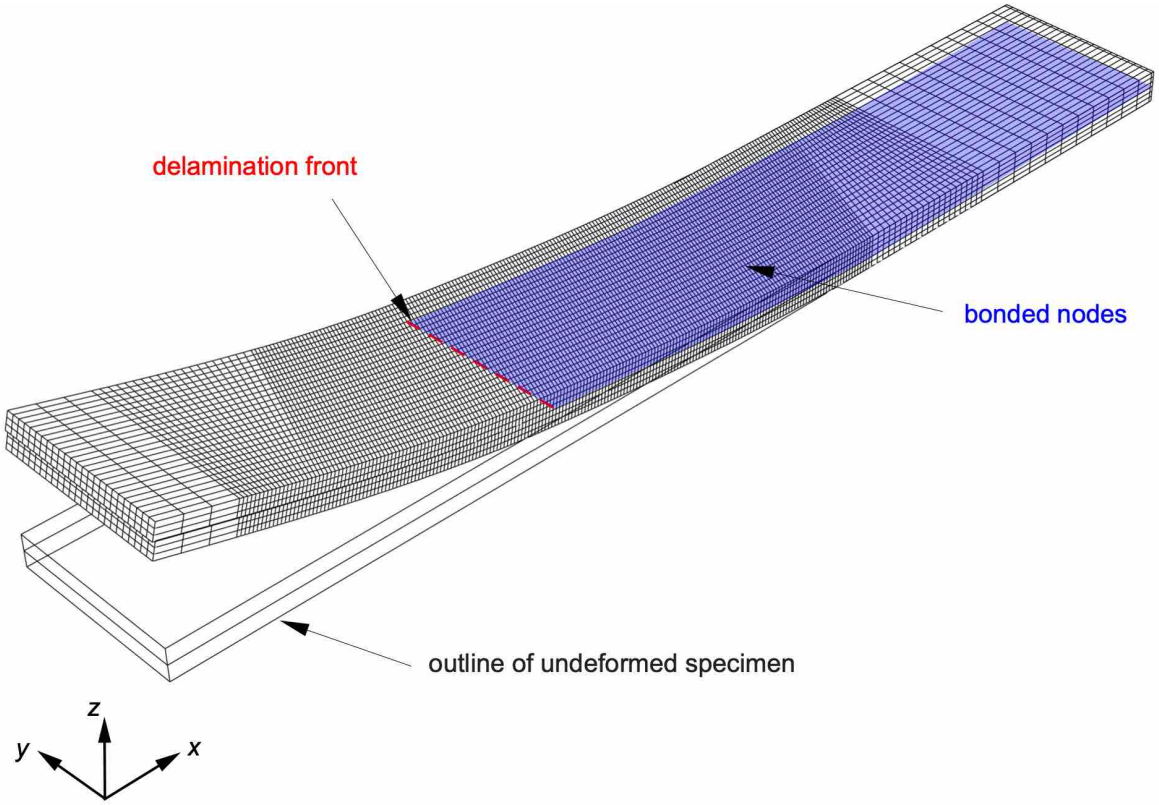

(a). *Mesh with element size Δa=0.5 mm in refined zone and ΔB=1.0 mm across the width.*

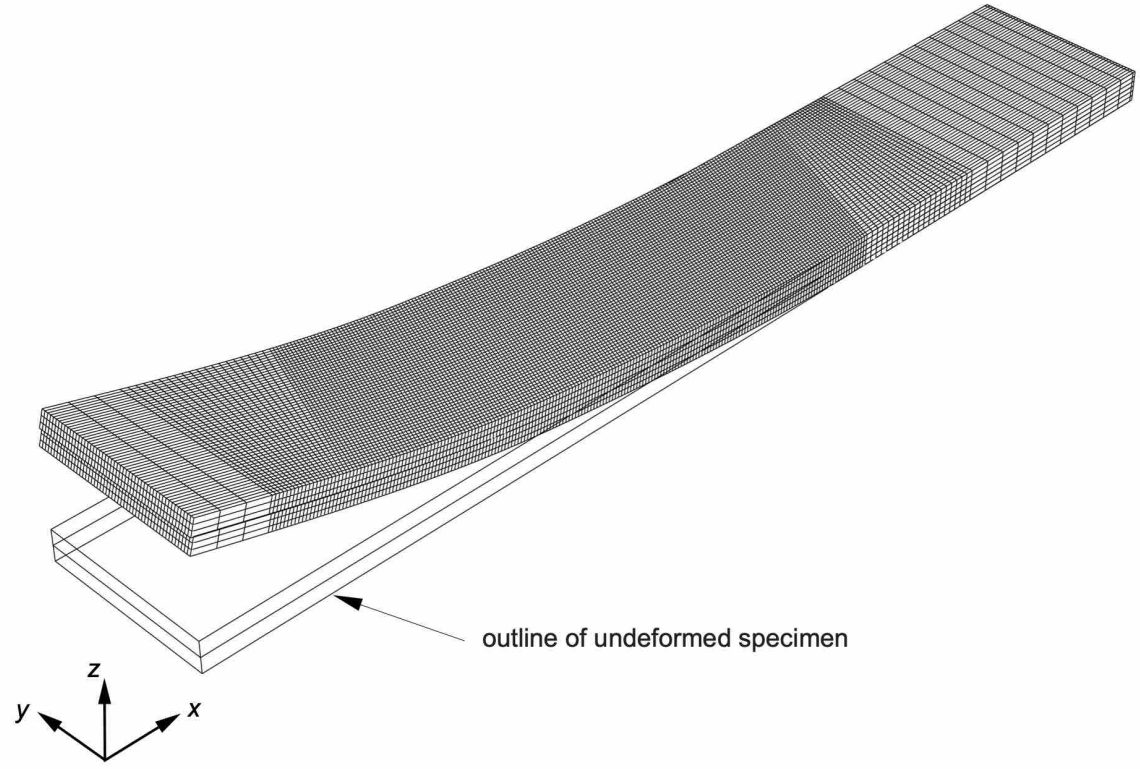

(b). *Mesh with element size Δa=0.5 mm in refined zone and ΔB=0.5 mm across the width.*

Figure 4. 3D finite element models of C-ELS specimen with misaligned mesh.

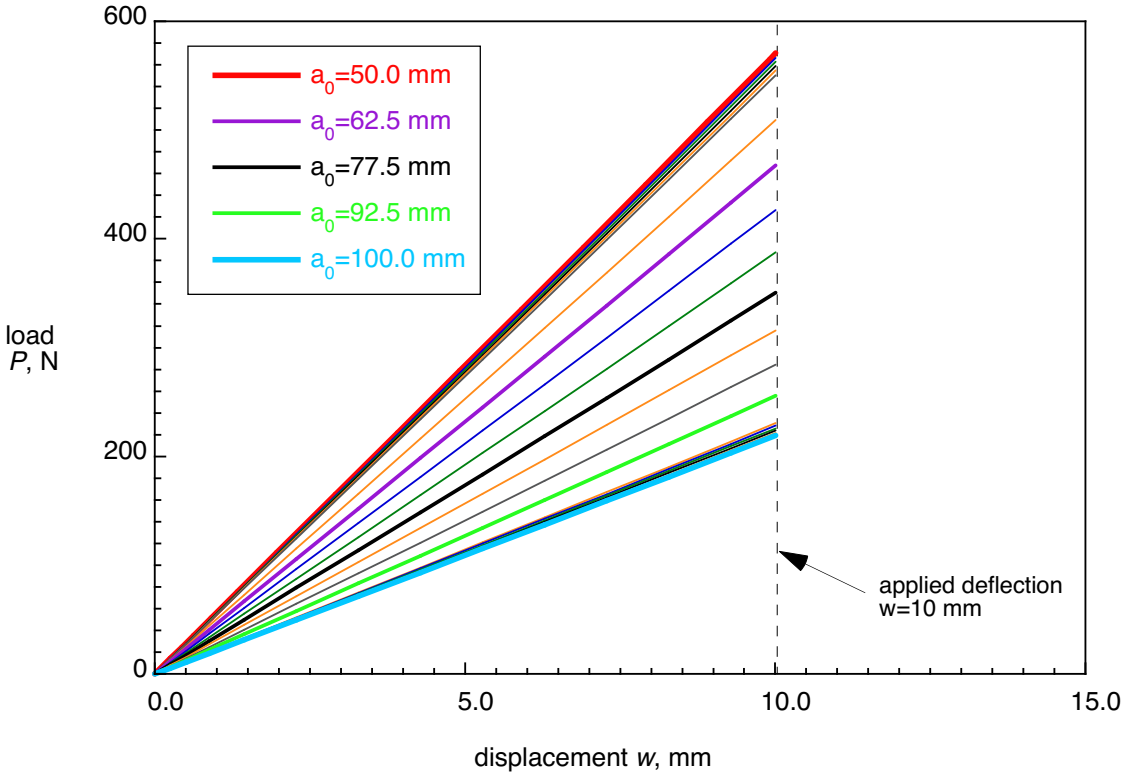

Figure 5. Computed load-displacement behavior of a C-ELS specimen for different delamination lengths a_0.

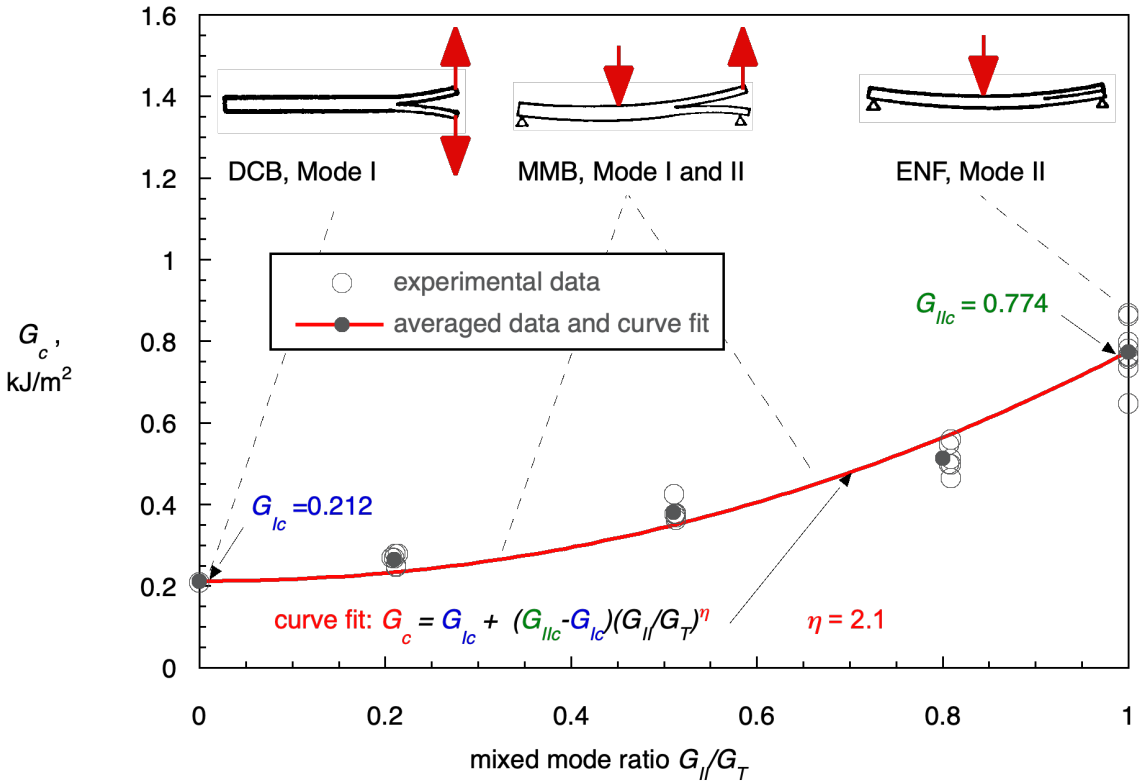

Figure 6. Mixed mode fracture criterion for IM7/8552 [21][22][23].

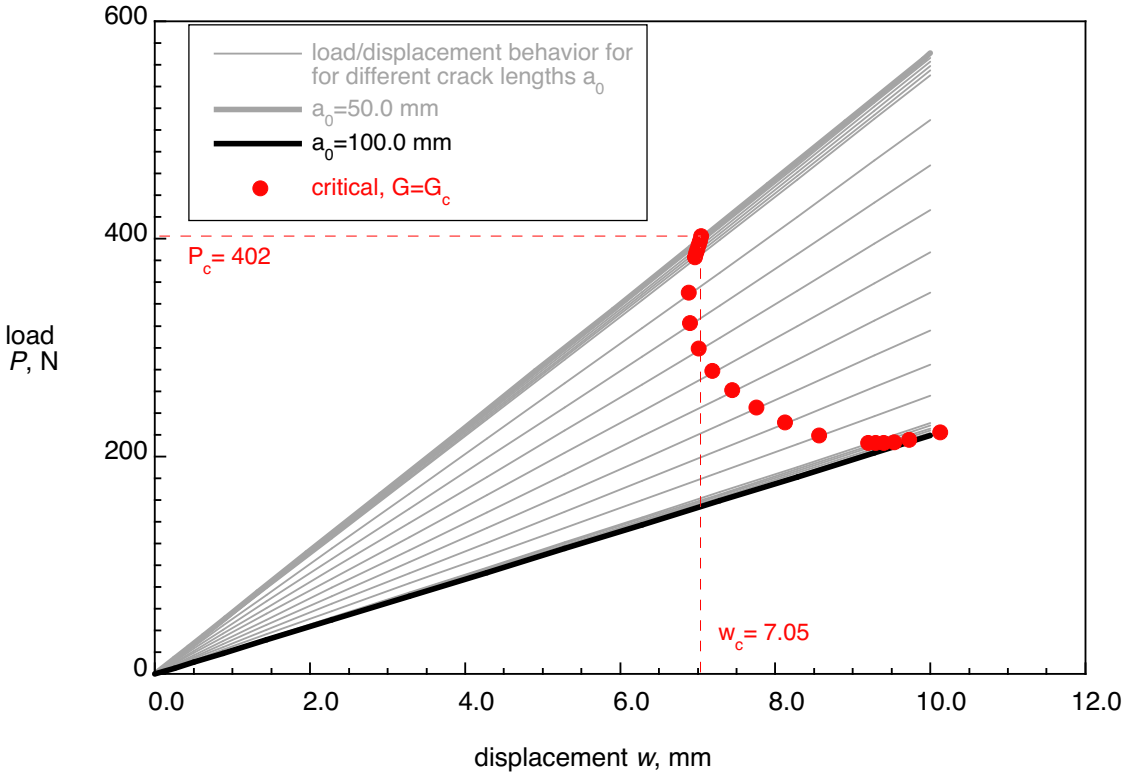

Figure 7. Computed load-displacement behavior of a C-ELS specimen for different delamination lengths a_0 and calculated critical behavior.

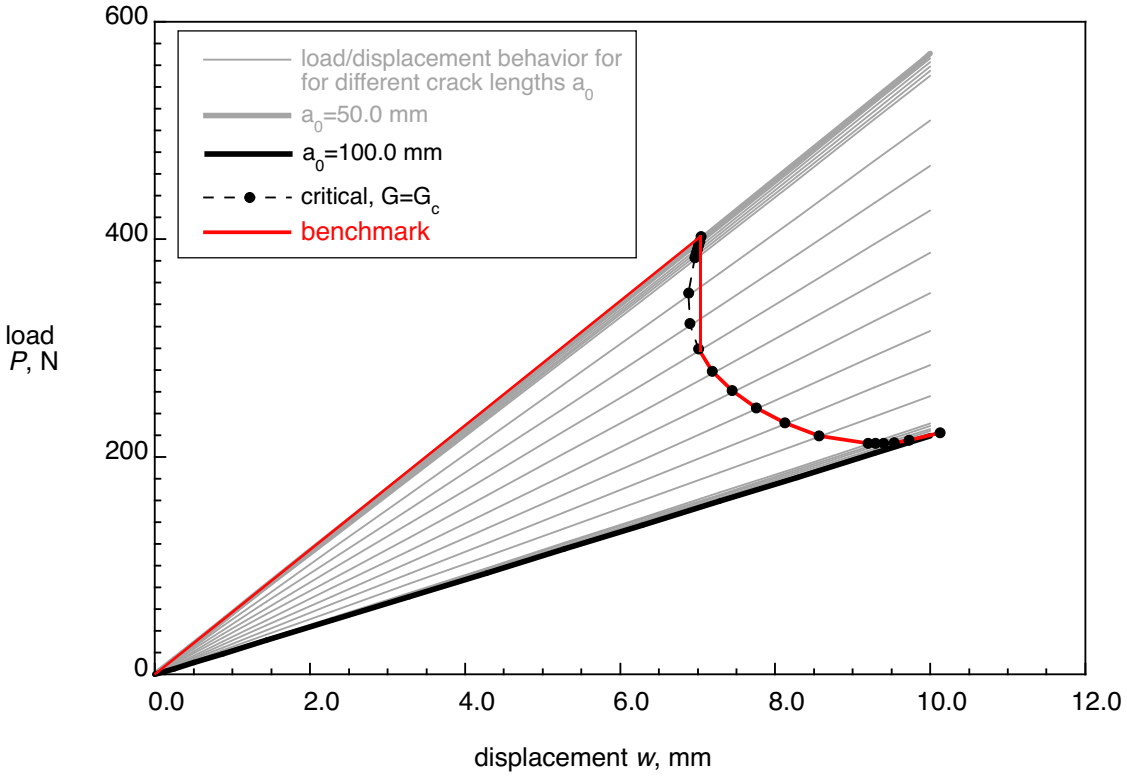

Figure 8. Computed load-displacement behavior of a C-ELS specimen for different delamination lengths a_0, calculated critical behavior and resulting benchmark case.

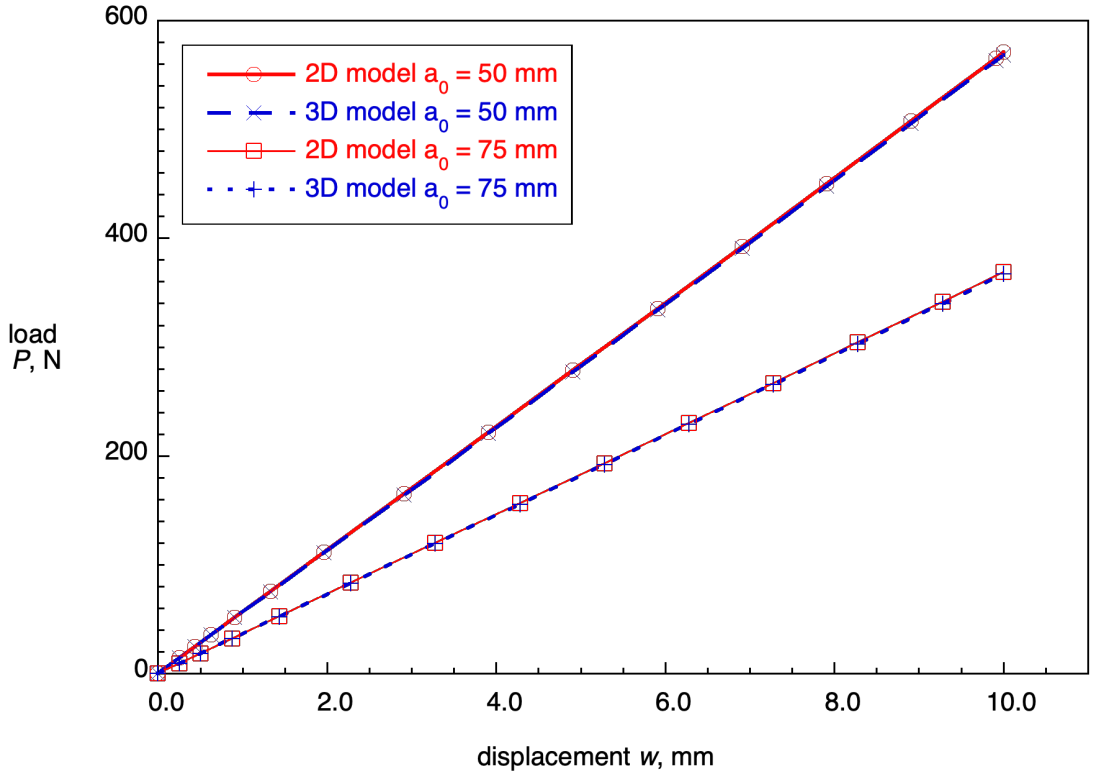

Figure 9. Comparison of computed load-displacement behavior of a C-ELS specimen obtained from 2D and 3D models for two different delamination lengths a_0.

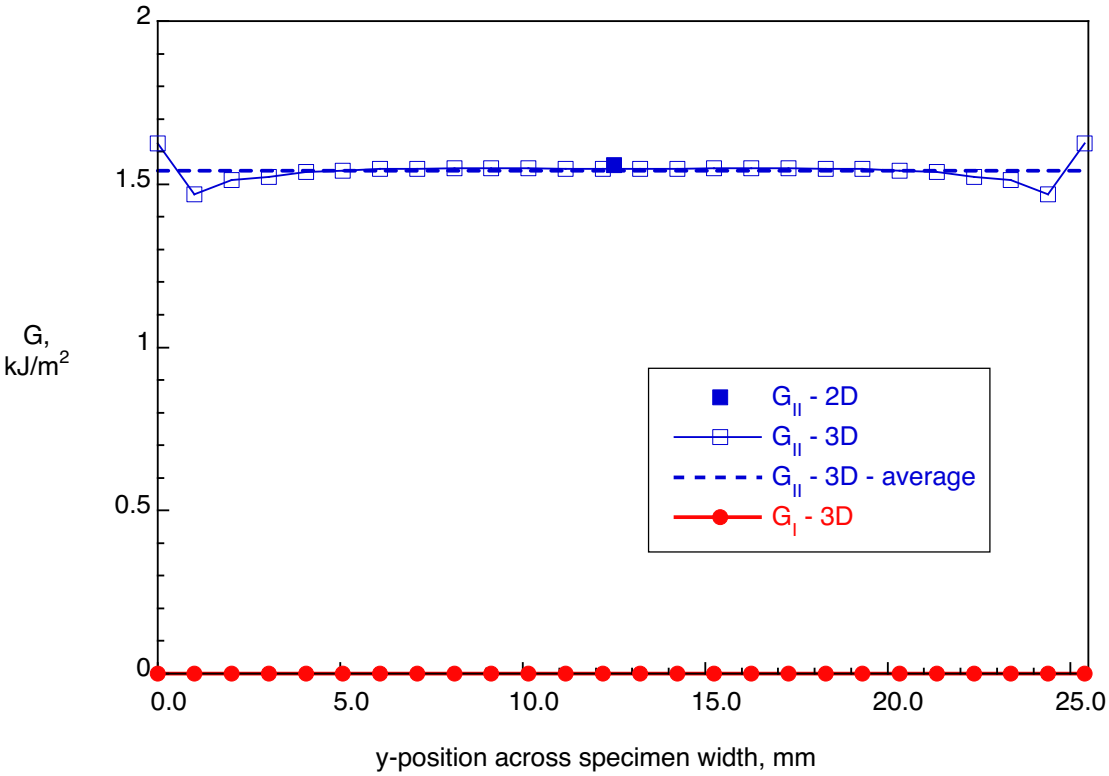

Figure 10. Energy release rate distribution across the width of a C-ELS specimen (a_0=50mm).

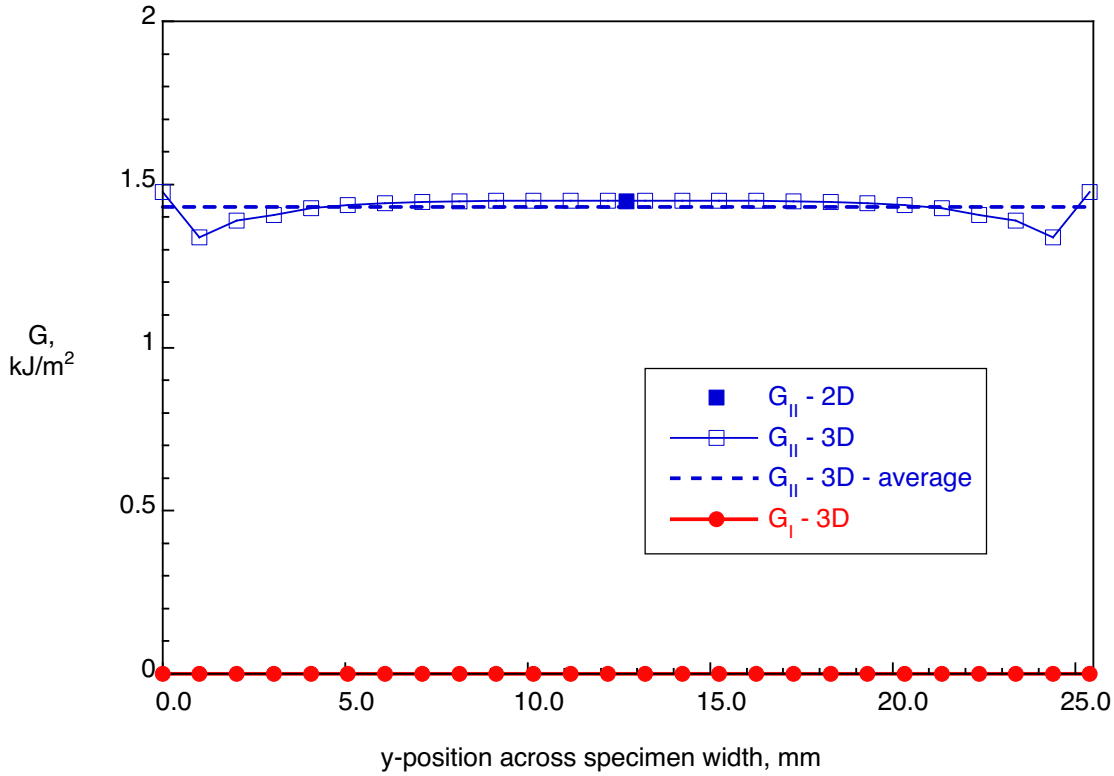

Figure 11. Energy release rate distribution across the width of a C-ELS specimen (a_0=75mm).

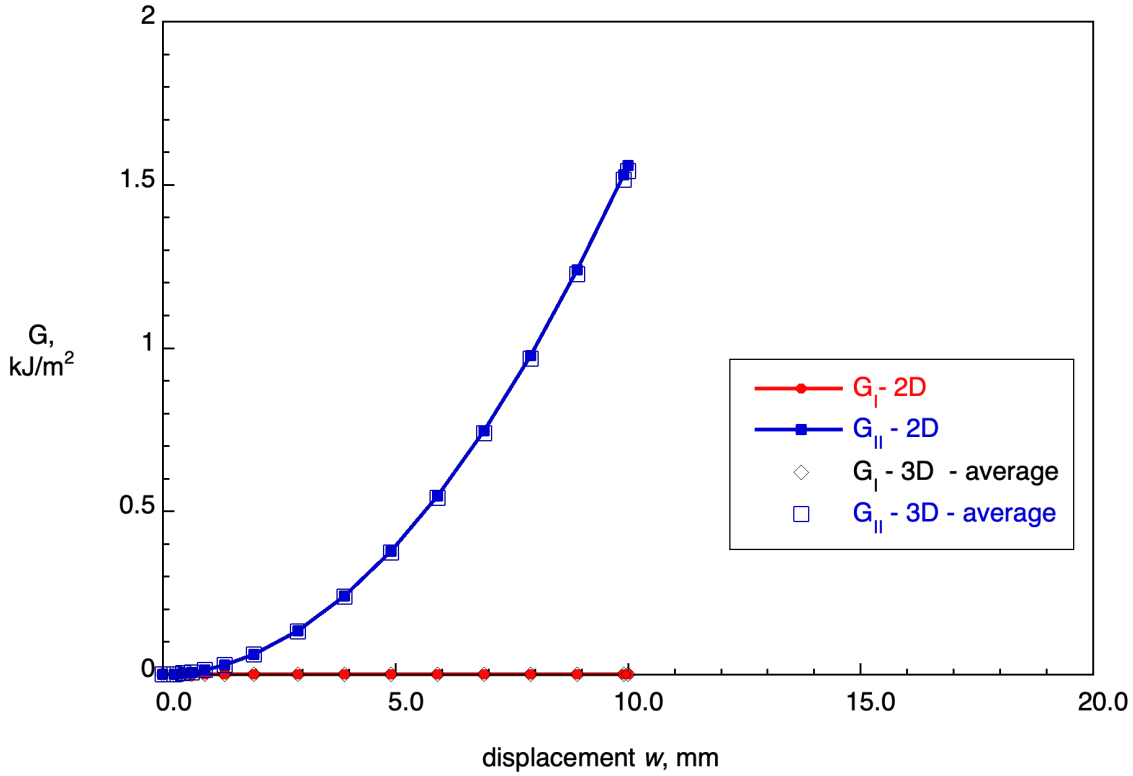

Figure 12. Energy release rate increase with increasing applied tip displacement (a_0=50mm).

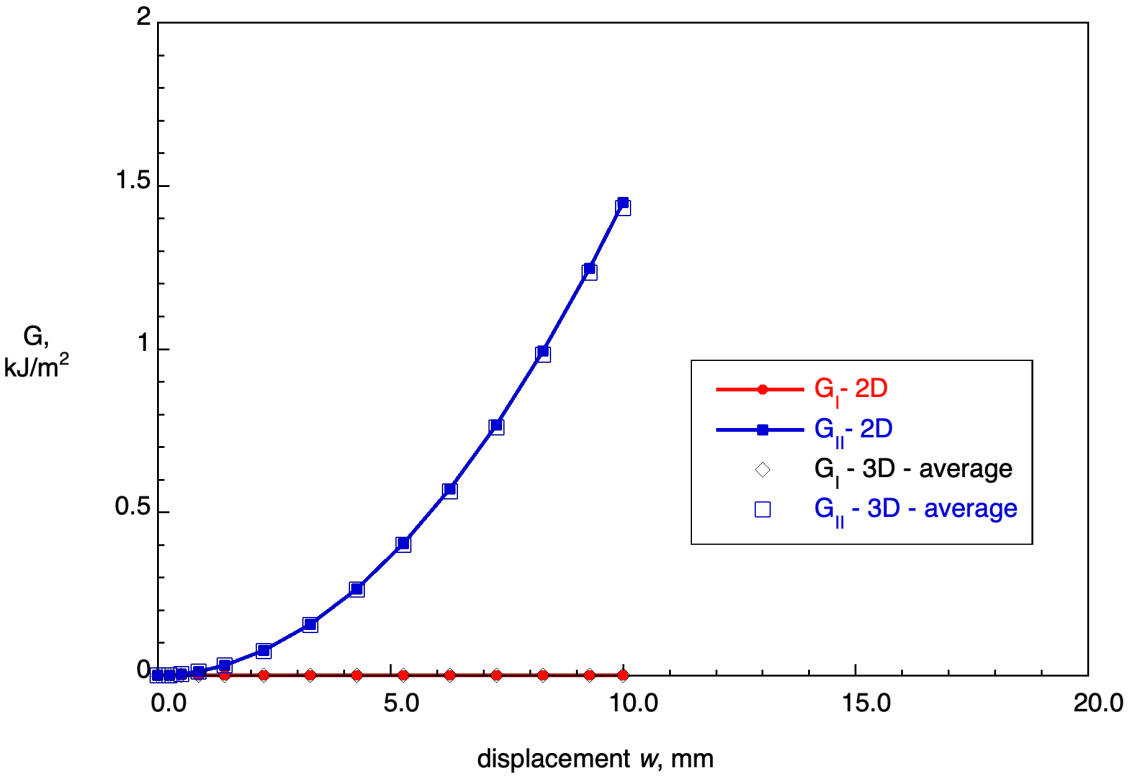

Figure 13. Energy release rate increase with increasing applied tip displacement (a_0=75mm).

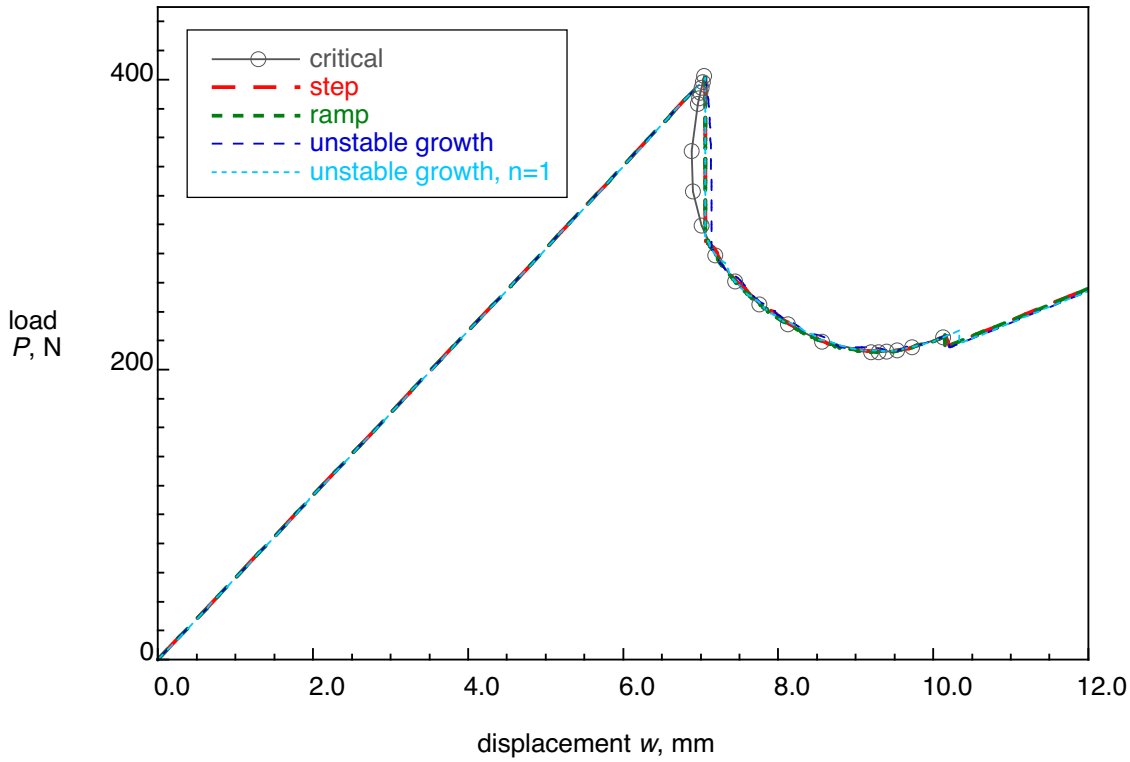

Figure 14. Computed load-displacement results obtained from automated propagation analyses using 2D FE models (a_0=50mm).

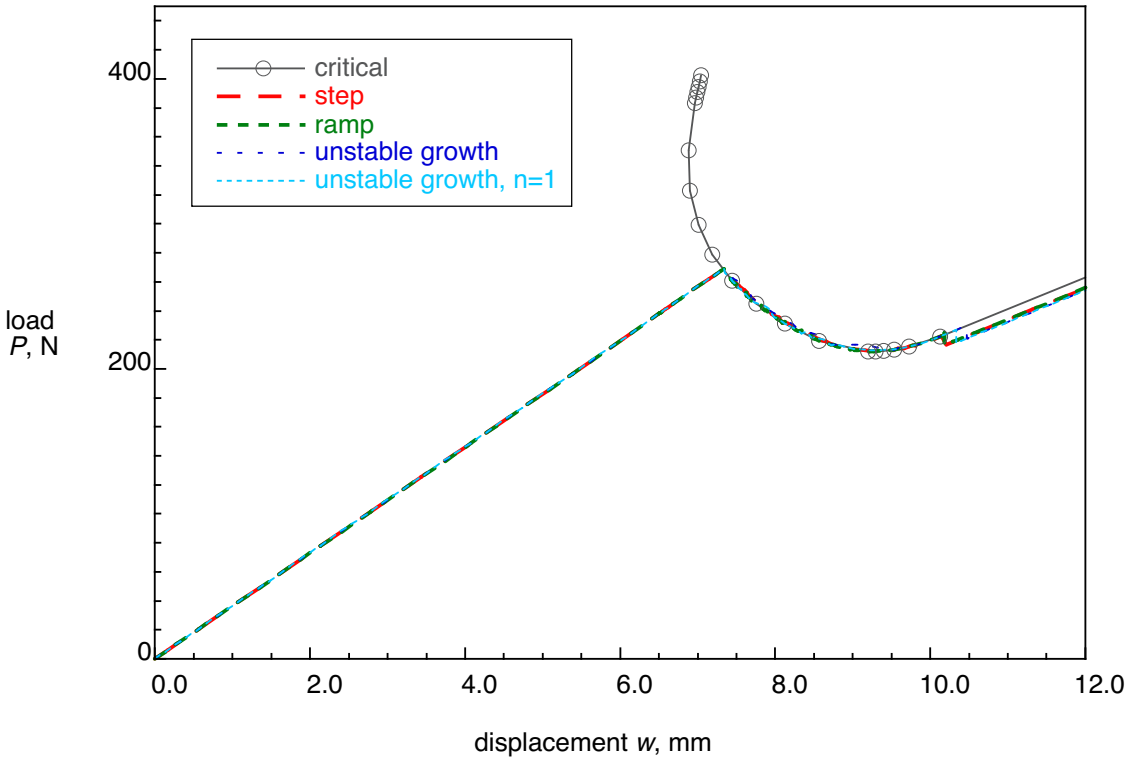

Figure 15. Computed load-displacement results obtained from automated propagation analyses using 2D FE models (a_0=75mm).

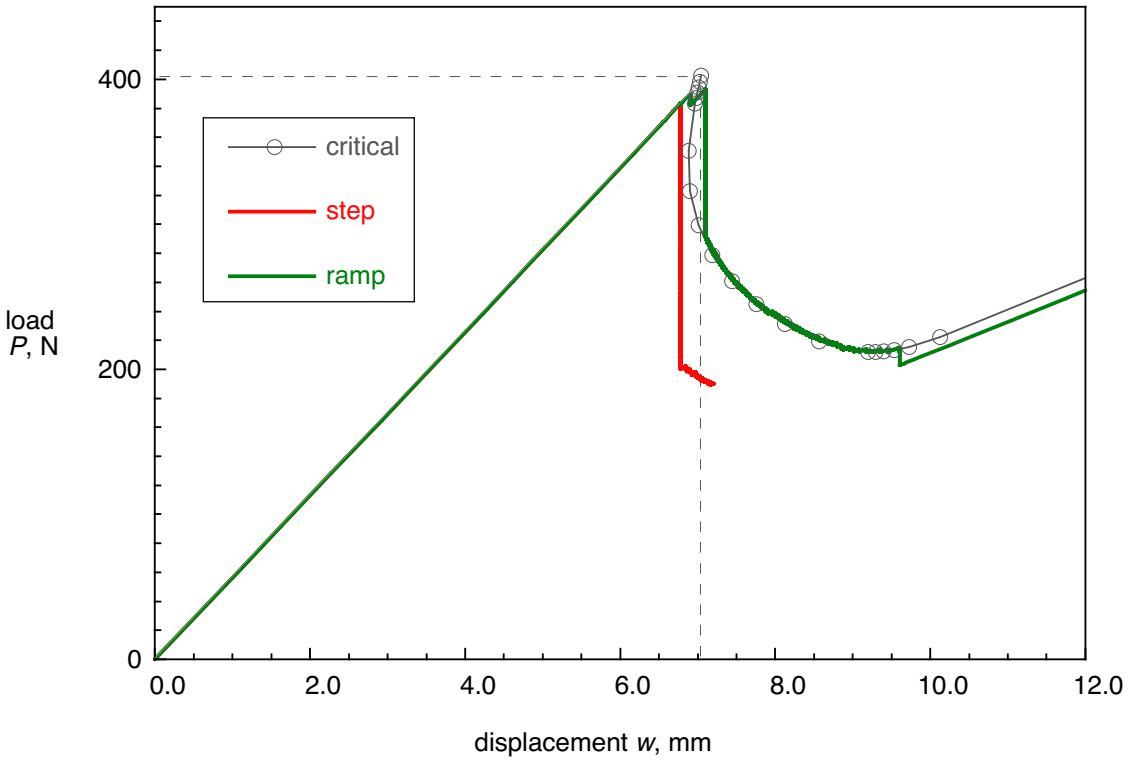

Figure 16. Load-displacement results obtained from automated propagation analyses using 3D models with aligned meshes and original input variables (a_0=50mm, ΔB=1.0mm).

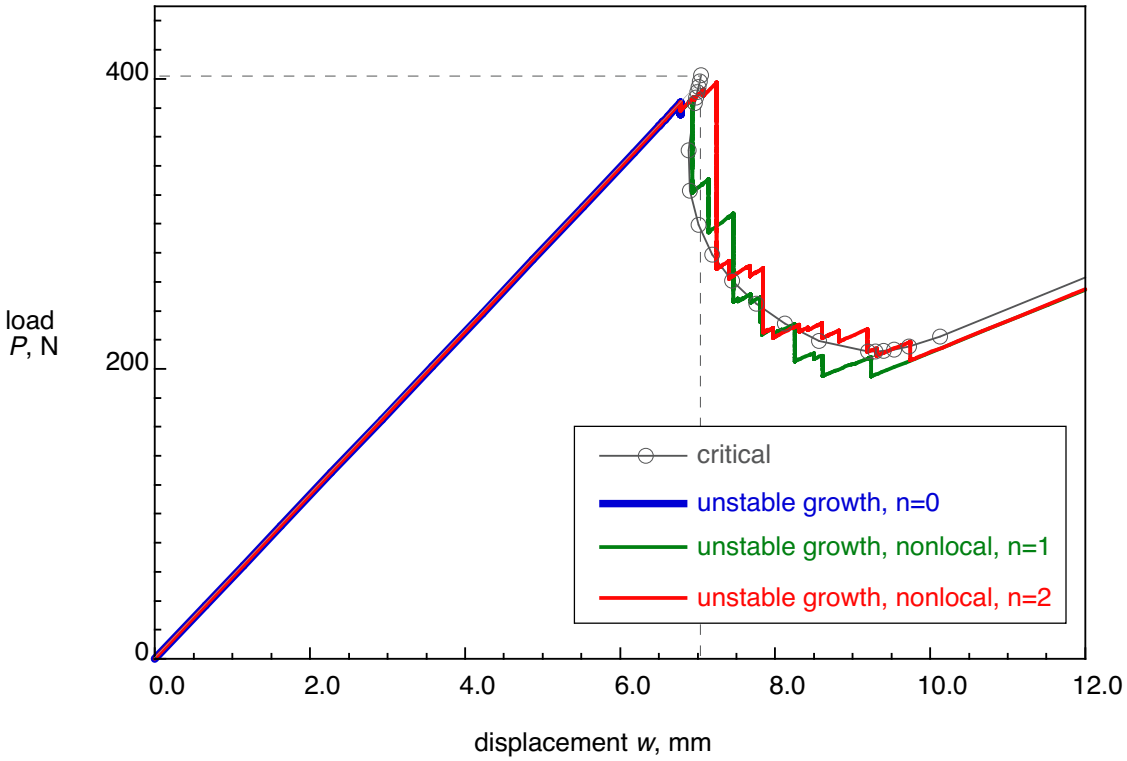

Figure 17. Load-displacement results obtained from automated propagation analyses using 3D models with aligned meshes and new input variables (a_0=50mm, ΔB=1.0mm).

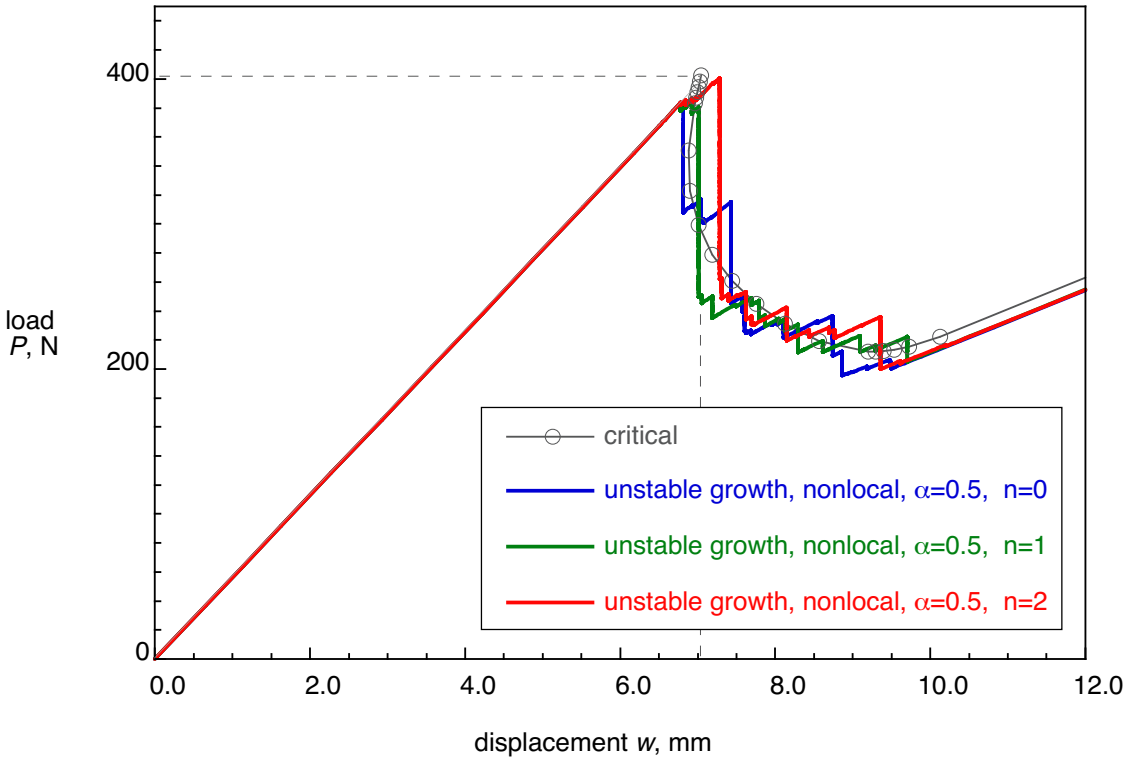

Figure 18. Load-displacement results obtained from automated propagation analyses using 3D models with aligned meshes and modified input variables (a_0=50mm, ΔB=1.0mm).

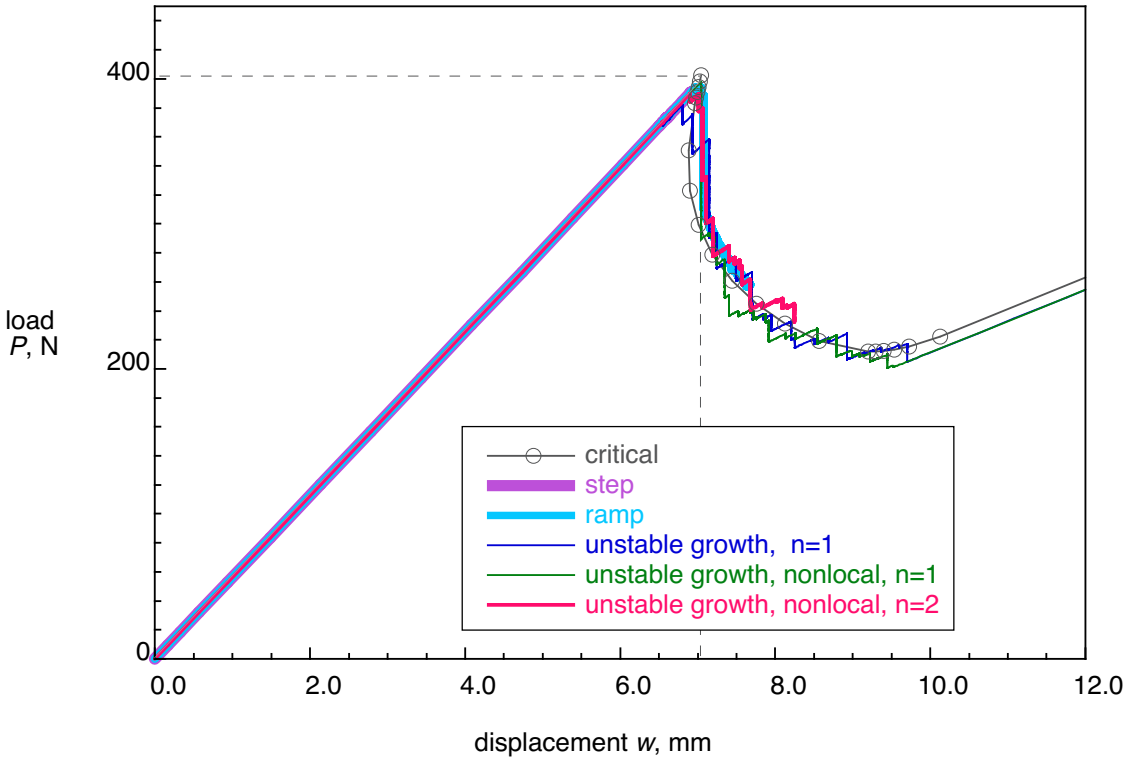

Figure 19. Load-displacement results obtained from automated propagation analyses using 3D models with aligned meshes and different input variables (a_0=50mm, ΔB=0.5mm).

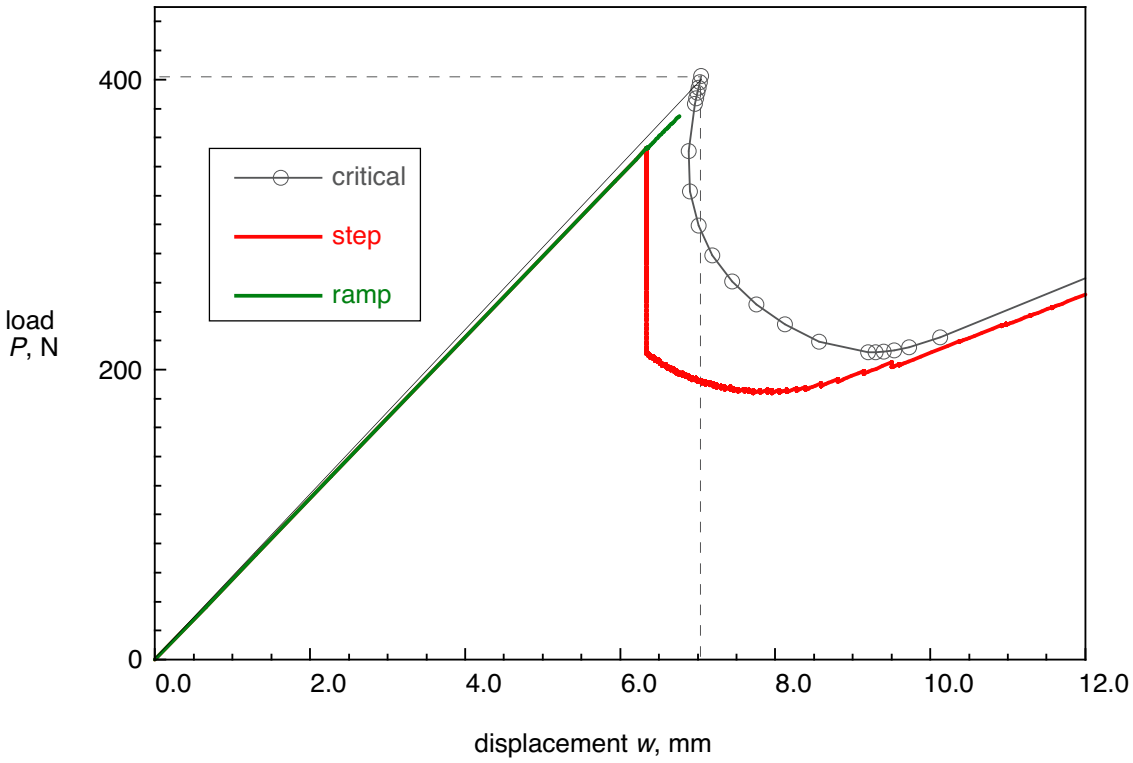

Figure 20. Computed load-displacement results obtained from automated propagation analyses using a 3D FE model with misaligned mesh and original input variables (a_0=50mm, ΔB=1.0mm).

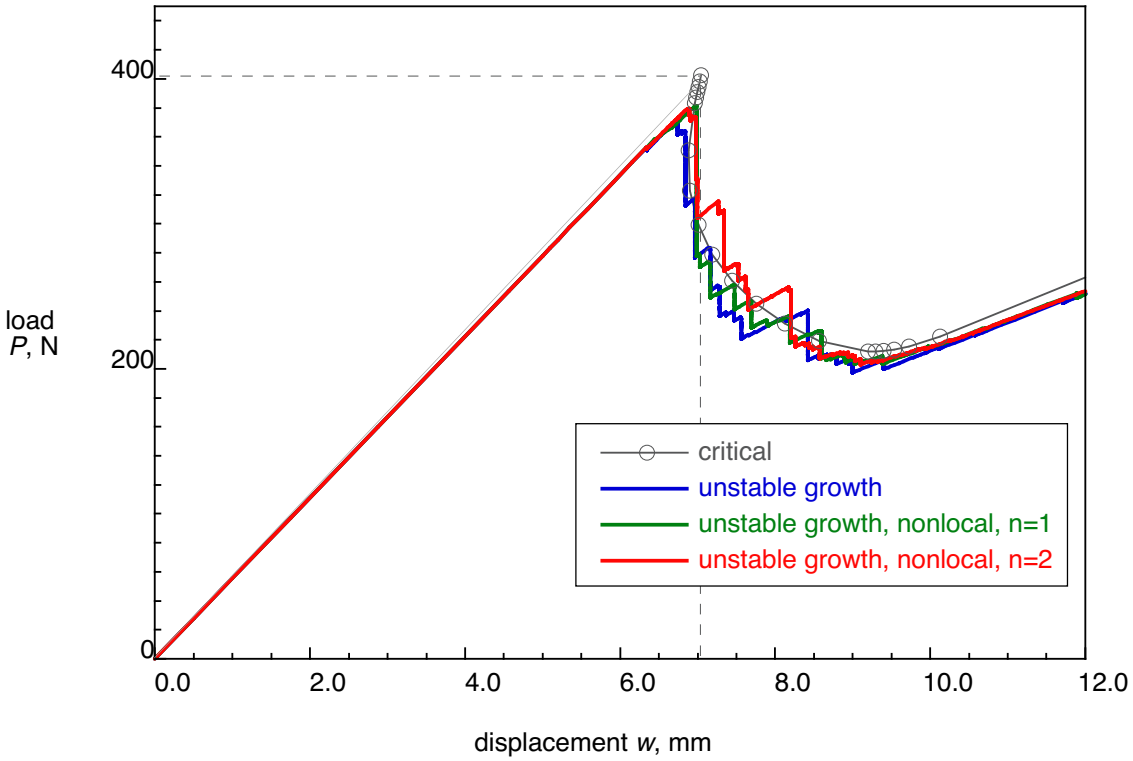

Figure 21. Computed load-displacement results obtained from automated propagation analyses using a 3D FE model with misaligned mesh and new input variables (a_0=50mm, ΔB=1.0mm).

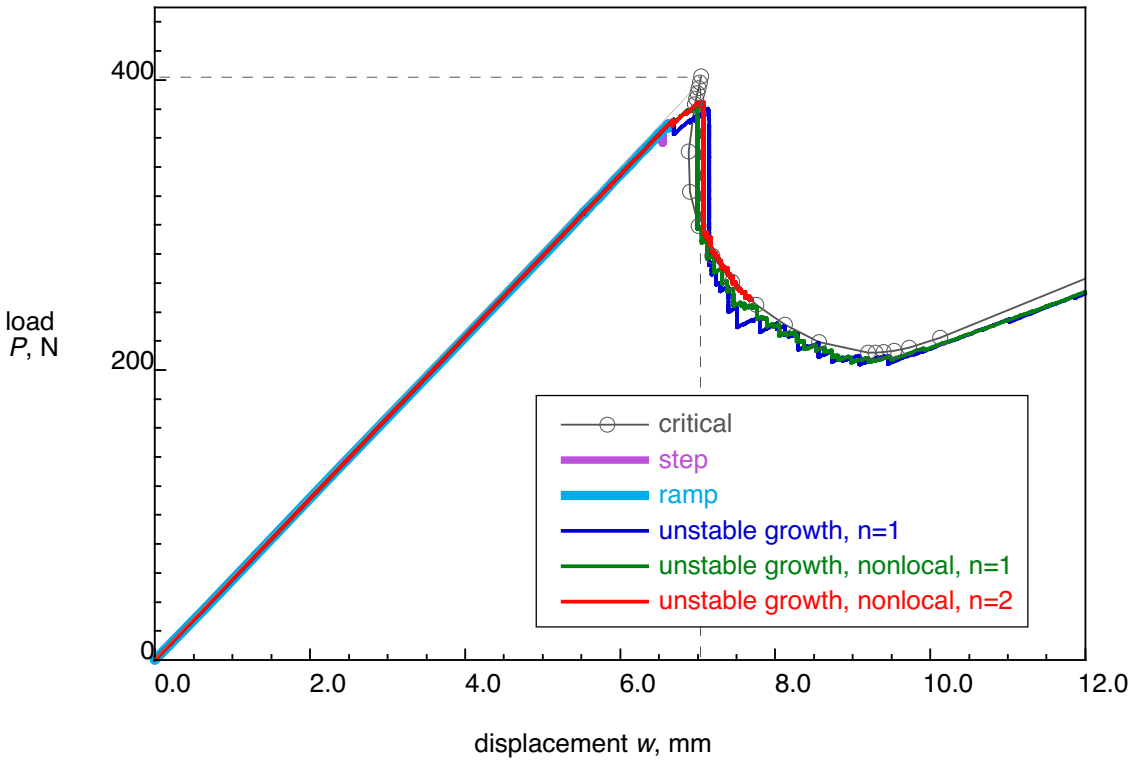

Figure 22. Computed load-displacement results obtained from automated propagation analyses using a 3D FE model with misaligned mesh and different input variables (a_0=50mm,ΔB=0.5mm).

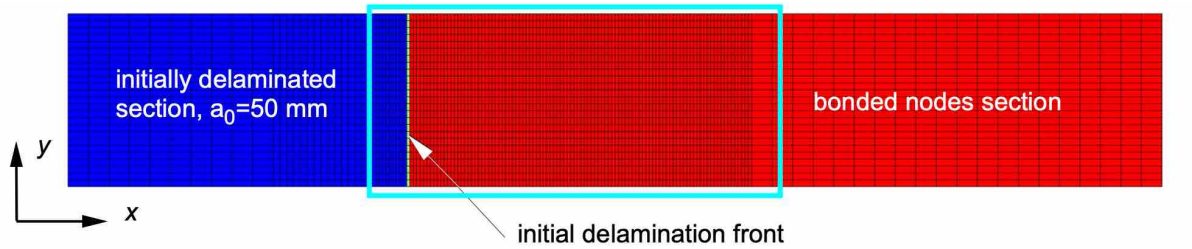

(a). *Location of delamination front at the beginning of the analyses (a_0=50 mm, ΔB=1.0 mm).*

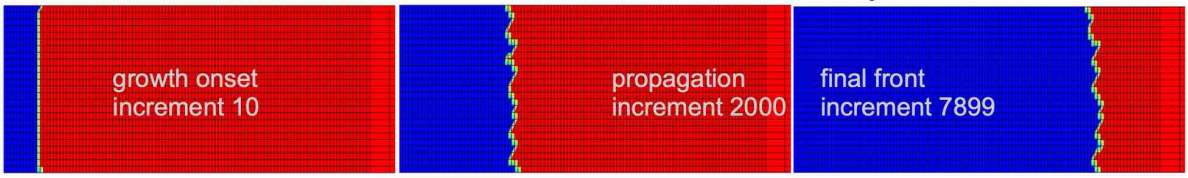

(b). *DEBONDING FORCE=STEP.*

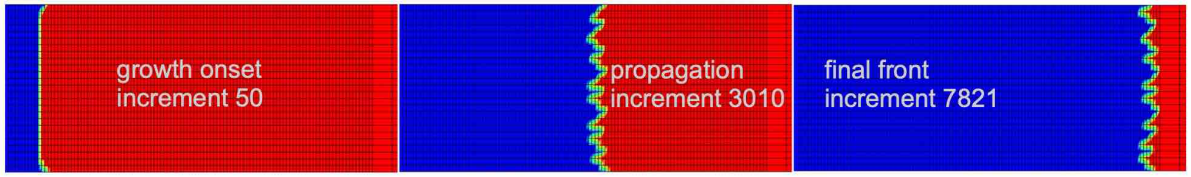

(c). *DEBONDING FORCE=RAMP.*

(d). *DEBONDING FORCE=RAMP, unstable growth tolerance, α=0.9, β=1E10, n=1.*

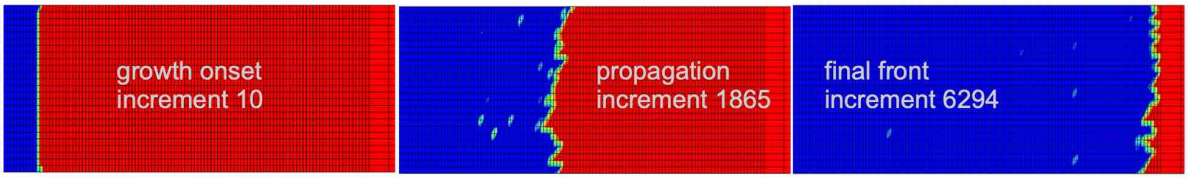

(e). *DEBONDING FORCE=RAMP, unstable growth tolerance, nonlocal, α=0.9, β=1E10, n=1.*

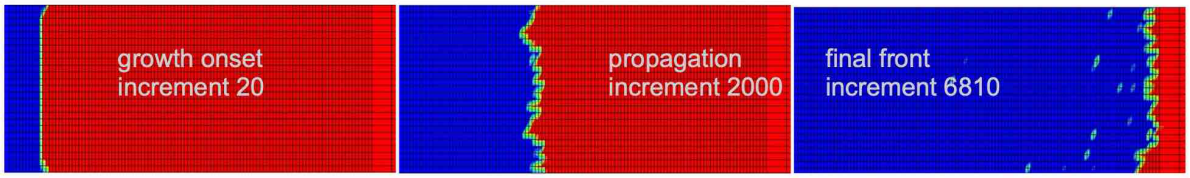

(f). *DEBONDING FORCE=RAMP, unstable growth tolerance, nonlocal, α=0.9, β=1E10, n=2.*

(g). *DEBONDING FORCE=RAMP, unstable growth tolerance, nonlocal, α=0.9, β=1E10, n=1 (ΔB=0.5 mm).*

Figure 23. Delamination front contours during automated VCCT-based propagation analysis obtained from 3D FE models with aligned meshes (a_0=50mm).

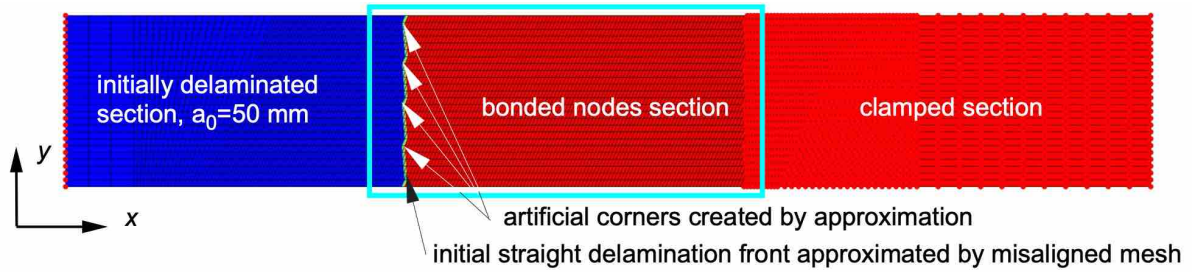

(a). *Location of delamination front at the beginning of the analyses (a_0=50 mm, ΔB=1.0 mm).*

(b). *DEBONDING FORCE=STEP.*

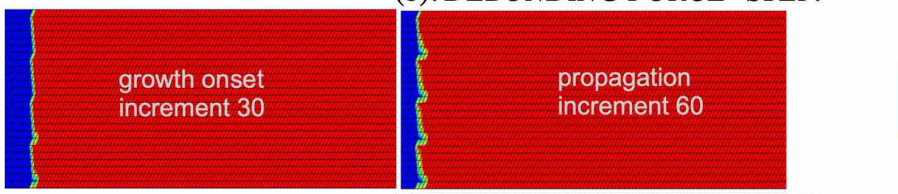

(c). *DEBONDING FORCE=RAMP.*

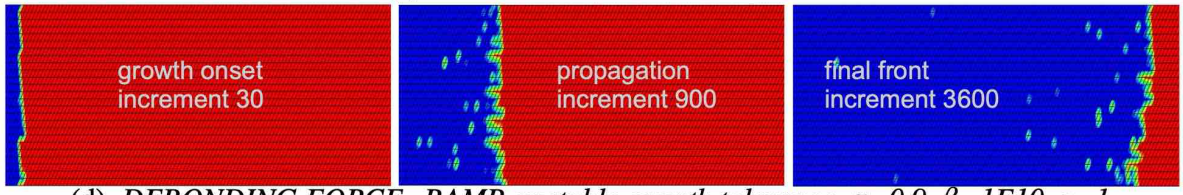

(d). *DEBONDING FORCE=RAMP, unstable growth tolerance, α=0.9, β=1E10, n=1.*

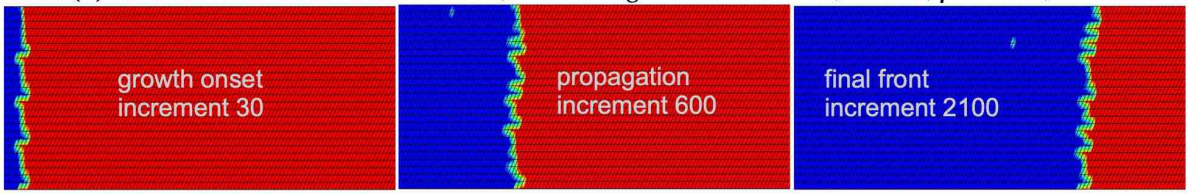

(e). *DEBONDING FORCE=RAMP, unstable growth tolerance, nonlocal, α=0.9, β=1E10, n=1.*

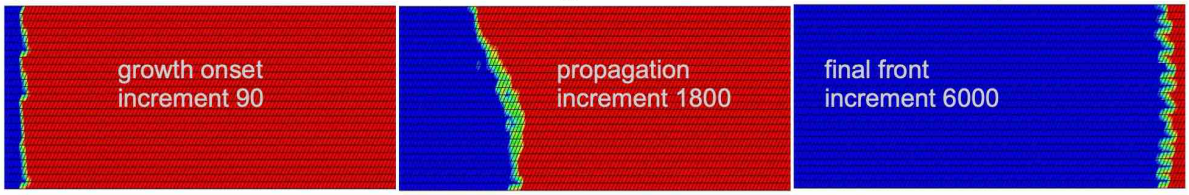

(f). *DEBONDING FORCE=RAMP, unstable growth tolerance, nonlocal, α=0.9, β=1E10, n=2.*

(g). *DEBONDING FORCE=RAMP, unstable growth tolerance, nonlocal, α=0.9, β=1E10, n=2 (ΔB=0.5 mm).*

Figure 24. Delamination front contours during automated VCCT-based propagation analysis obtained from 3D FE models with misaligned meshes (a_0=50mm).

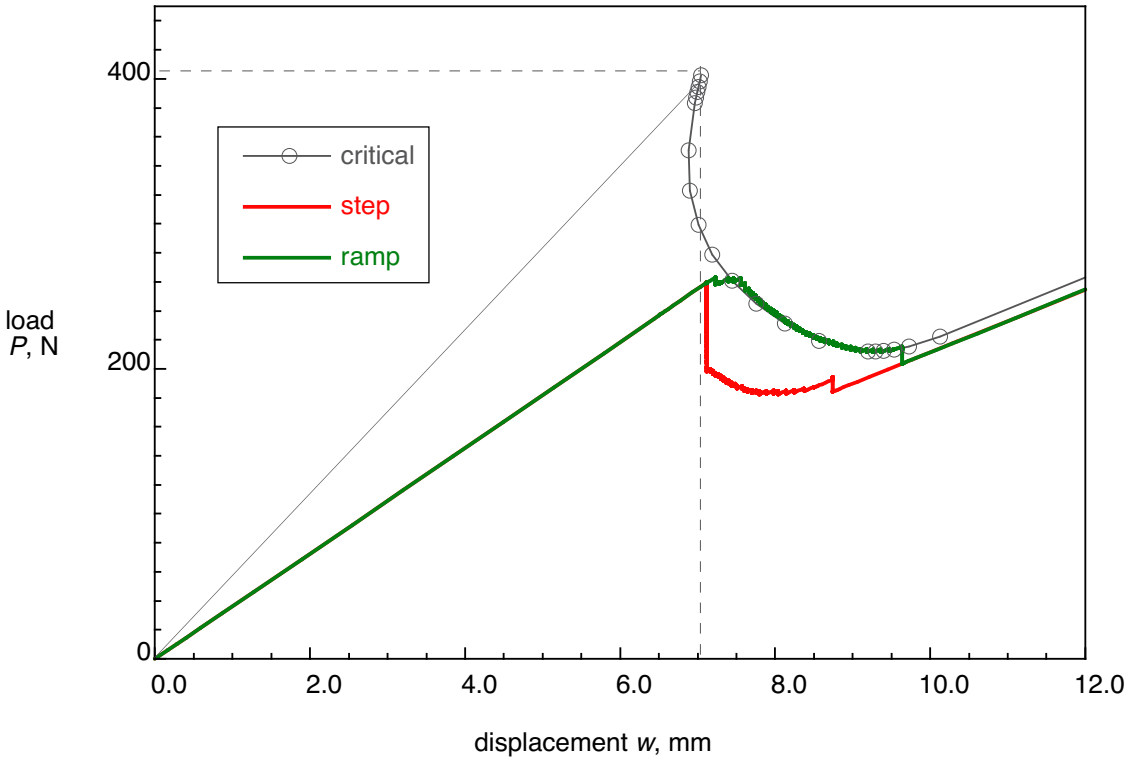

Figure 25. Load-displacement results obtained from automated propagation analyses using 3D models with aligned meshes and original input variables (a_0=75mm, ΔB=1.0mm).

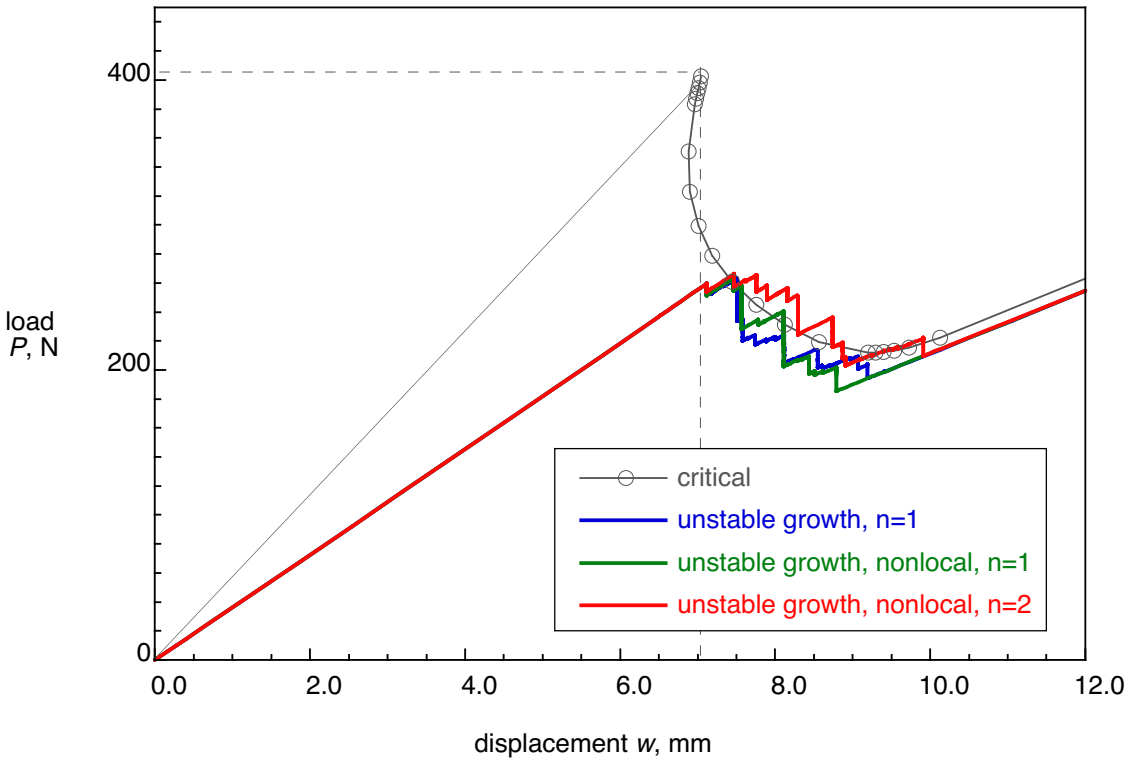

Figure 26. Load-displacement results obtained from automated propagation analyses using 3D models with aligned meshes and new input variables (a_0=75mm, ΔB=1.0mm).

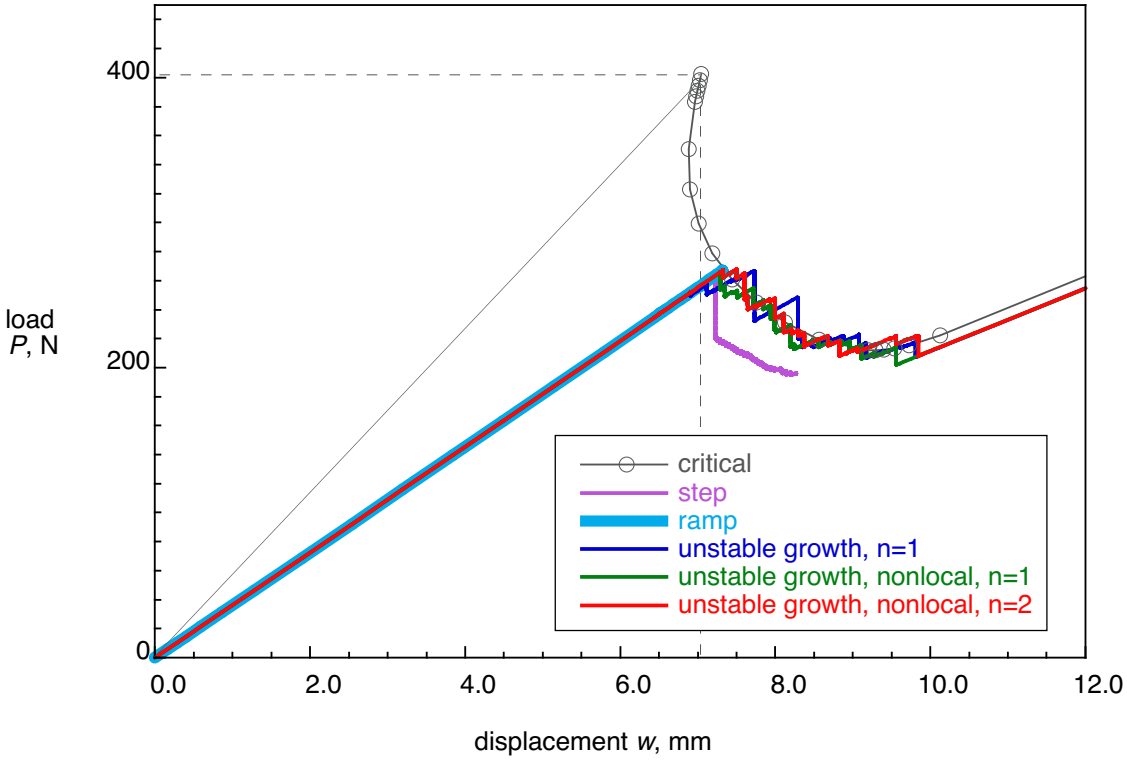

Figure 27. Load-displacement results obtained from automated propagation analyses using 3D models with aligned meshes and different input variables (a_0=75mm, ΔB=0.5mm).

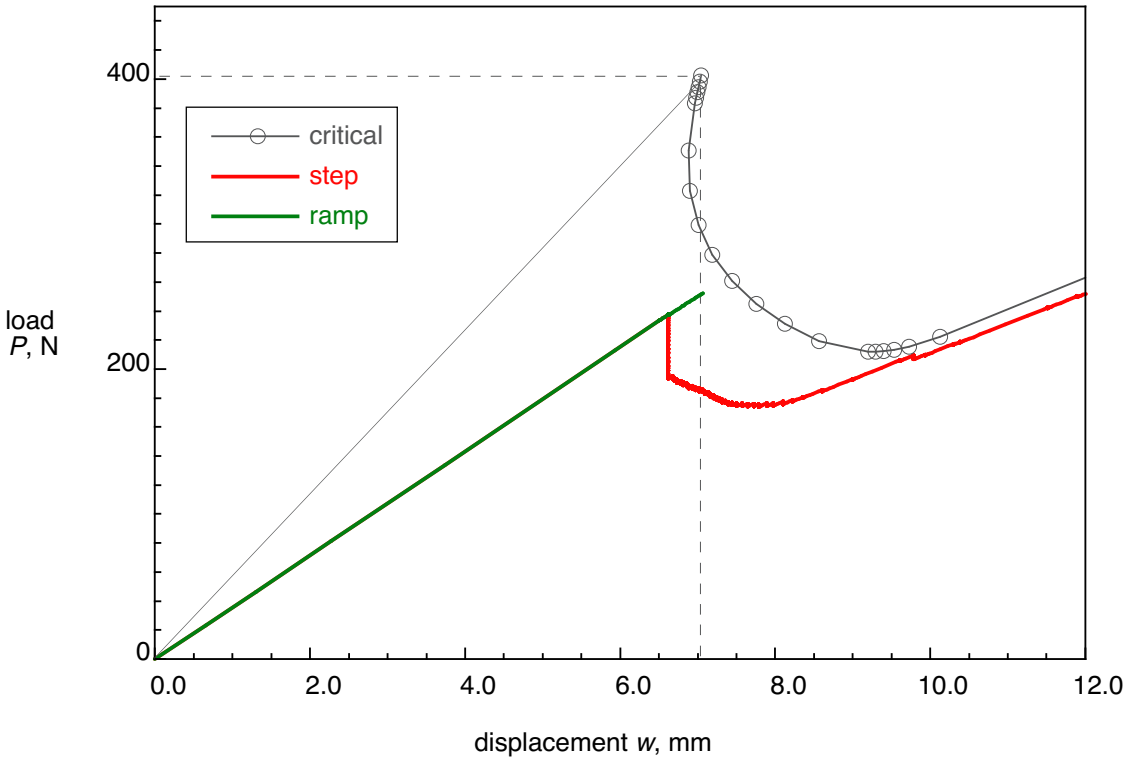

Figure 28. Computed load-displacement results obtained from automated propagation analyses using a 3D FE model with misaligned mesh and original input variables (a_0=75mm, ΔB=1.0mm).

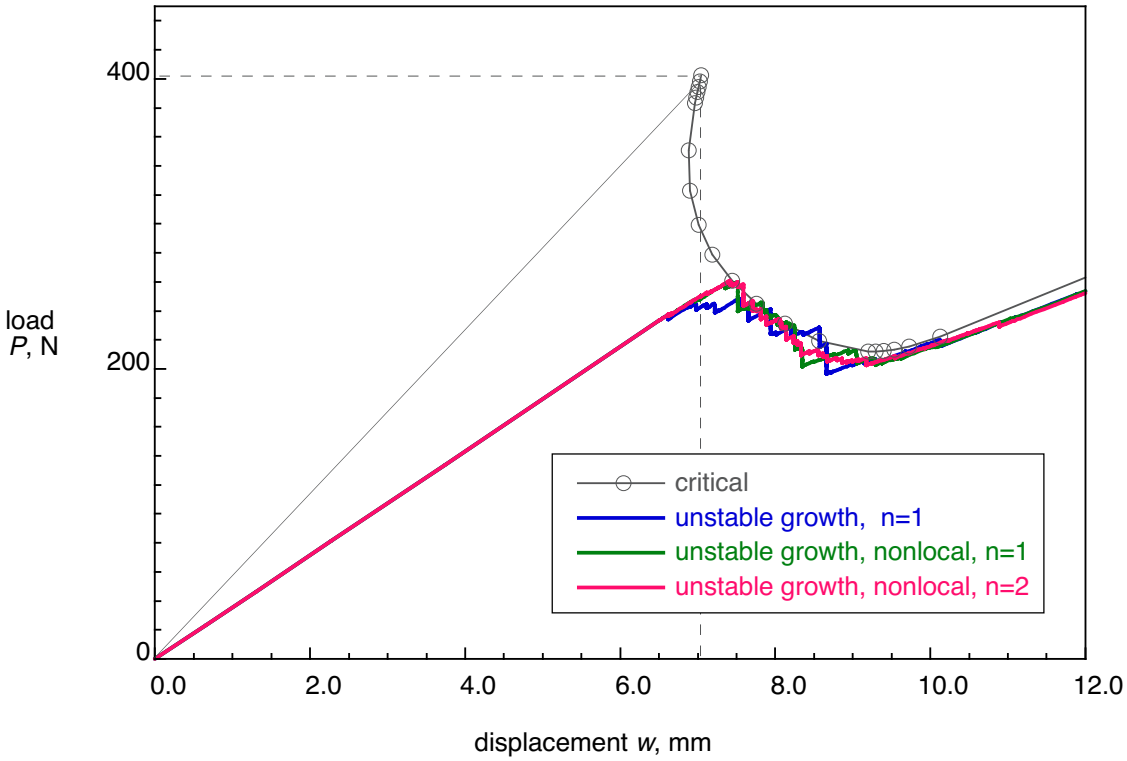

Figure 29. Computed load-displacement results obtained from automated propagation analyses using a 3D FE model with misaligned mesh and new input variables (a_0=75mm, ΔB=1.0mm).

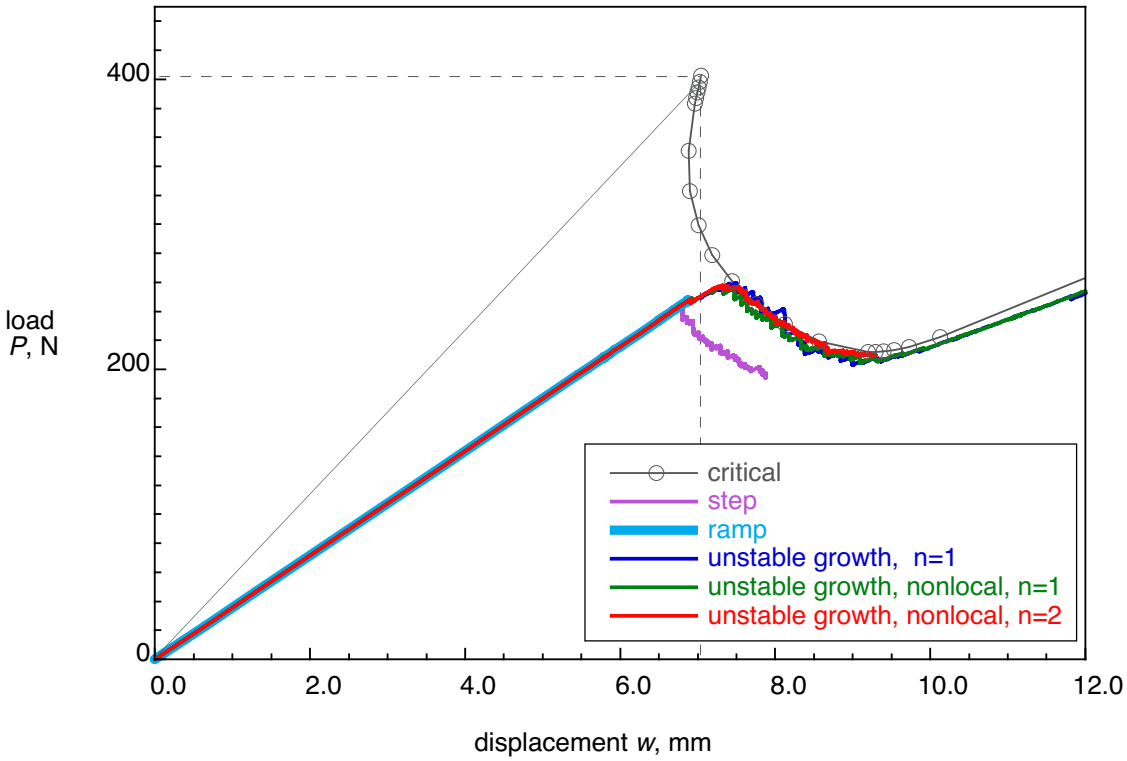

Figure 30. Computed load-displacement results obtained from automated propagation analyses using a 3D FE model with misaligned mesh and different input variables (a_0=75mm,ΔB=0.5mm)

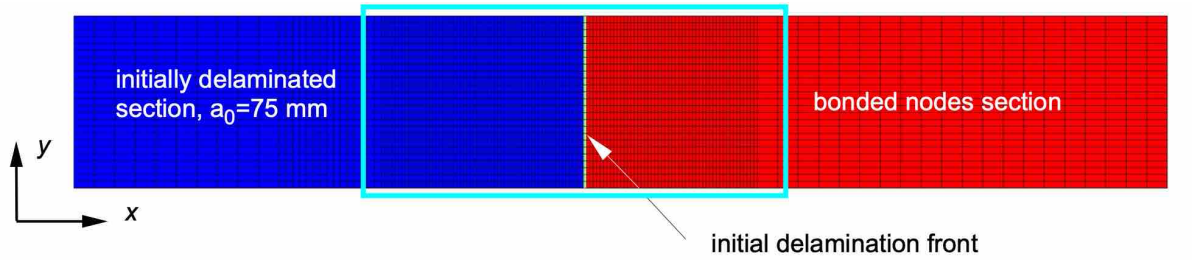

(a). *Location of delamination front at the beginning of the analyses (a_0=75 mm, ΔB=1.0 mm).*

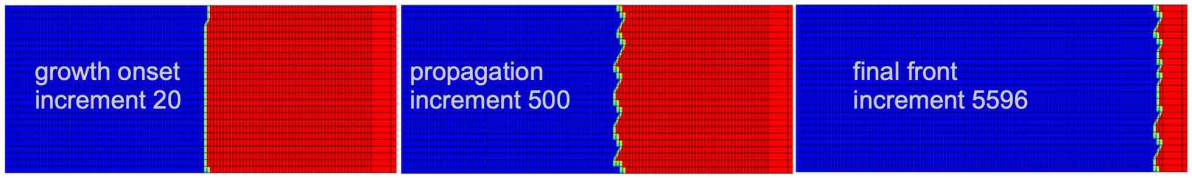

(b). *DEBONDING FORCE=STEP.*

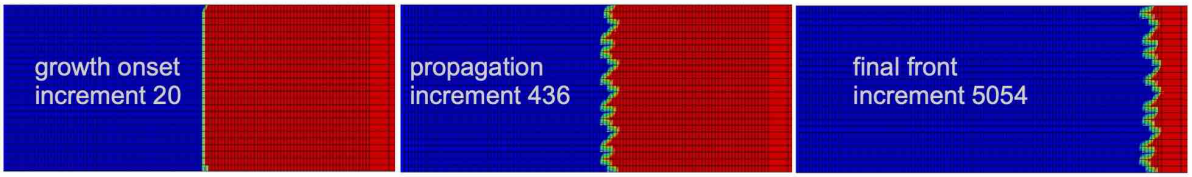

(c). *DEBONDING FORCE=RAMP.*

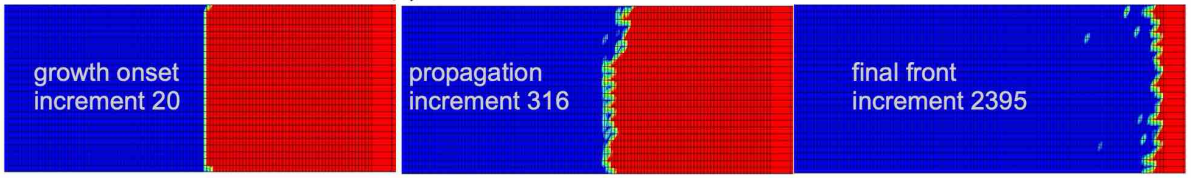

(d). *DEBONDING FORCE=RAMP, unstable growth tolerance, α=0.9, β=1E10, n=1.*

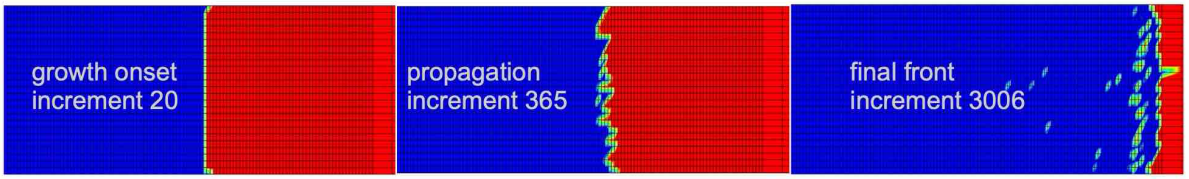

(e). *DEBONDING FORCE=RAMP, unstable growth tolerance, nonlocal, α=0.9, β=1E10, n=1.*

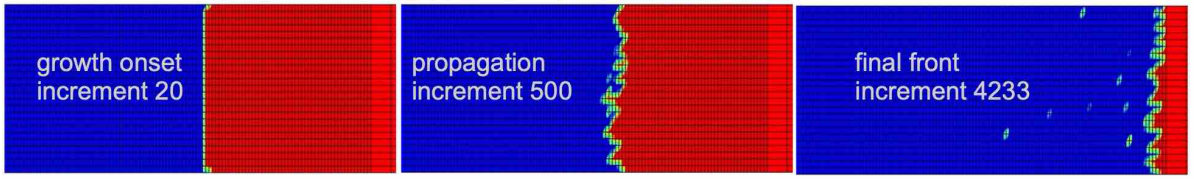

(f). *DEBONDING FORCE=RAMP, unstable growth tolerance, nonlocal, α=0.9, β=1E10, n=2.*

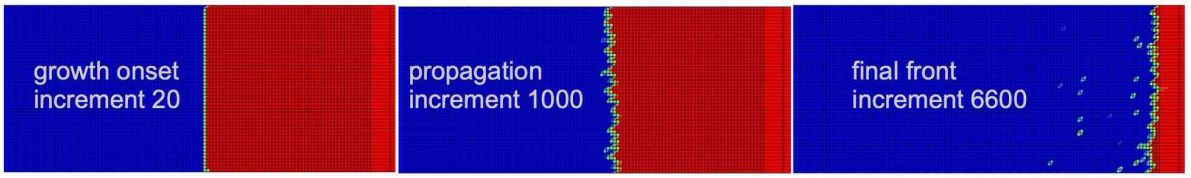

(g). *DEBONDING FORCE=RAMP, unstable growth tolerance, nonlocal, α=0.9, β=1E10, n=2 (ΔB=0.5 mm).*

Figure 31. Delamination front contours during automated VCCT-based propagation analysis obtained from 3D FE models with aligned meshes (a_0=75mm).

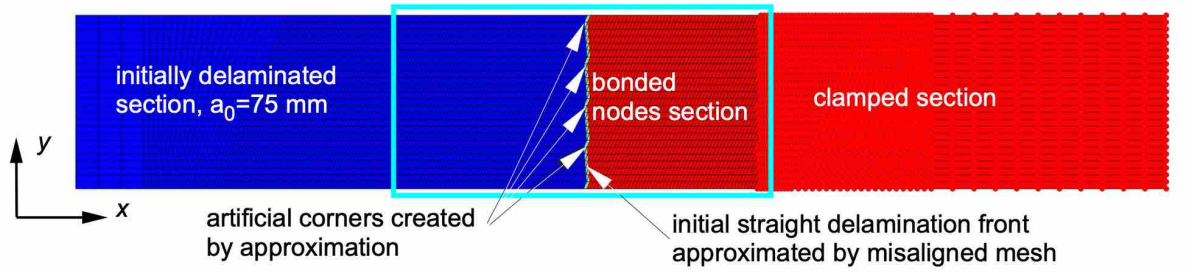

(a). *Location of delamination front at the beginning of the analyses (a_0=75 mm, ΔB=1.0 mm).*

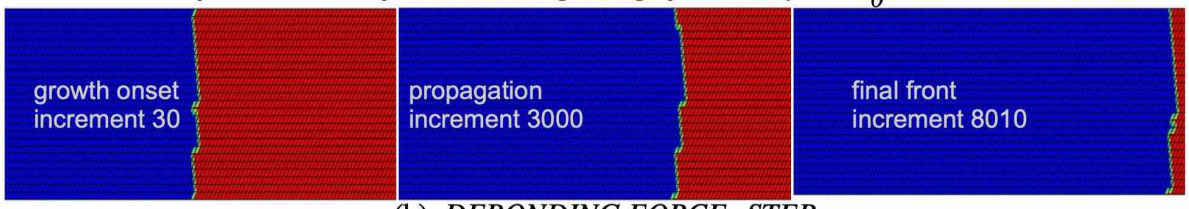

(b). *DEBONDING FORCE=STEP.*

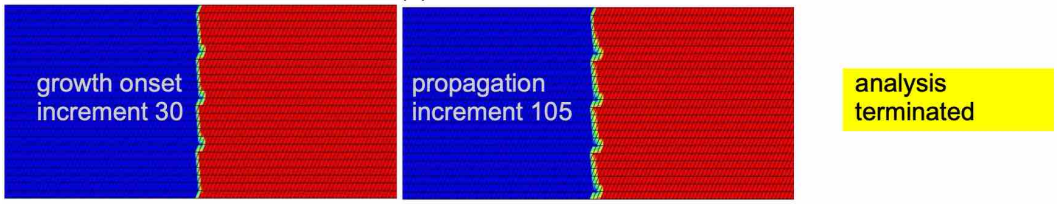

(c). *DEBONDING FORCE=RAMP.*

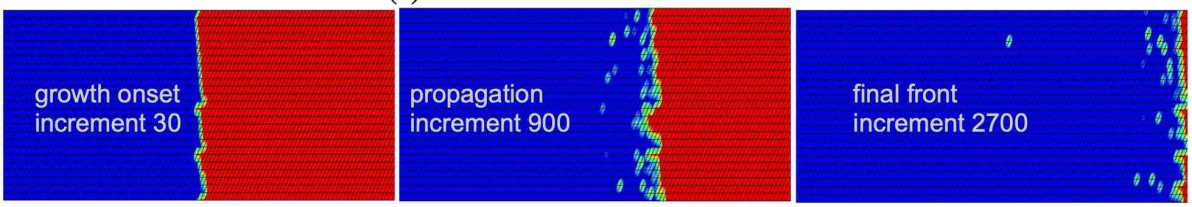

(d). *DEBONDING FORCE=RAMP, unstable growth tolerance, α=0.9, β=1E10, n=1.*

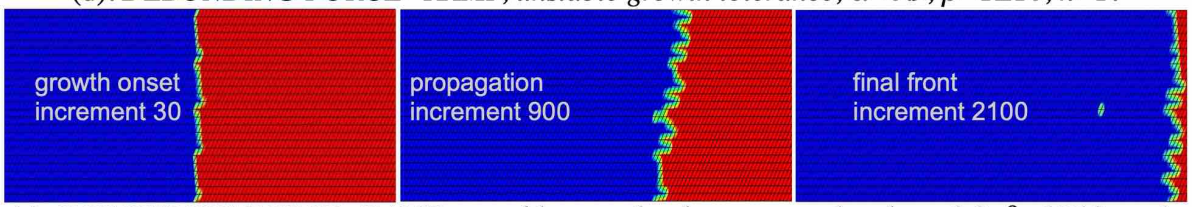

(e). *DEBONDING FORCE=RAMP, unstable growth tolerance, nonlocal, α=0.9, β=1E10, n=1.*

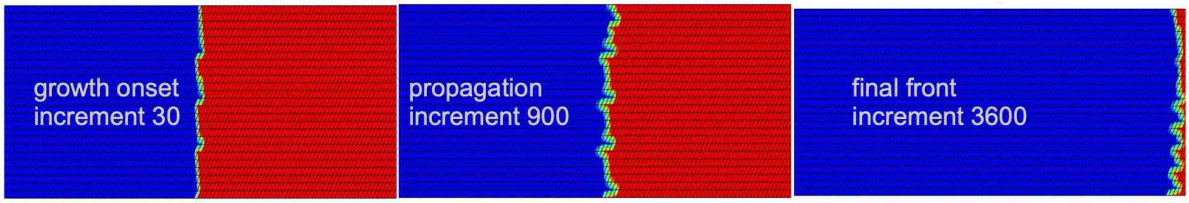

(f). *DEBONDING FORCE=RAMP, unstable growth tolerance, nonlocal, α=0.9, β=1E10, n=2.*

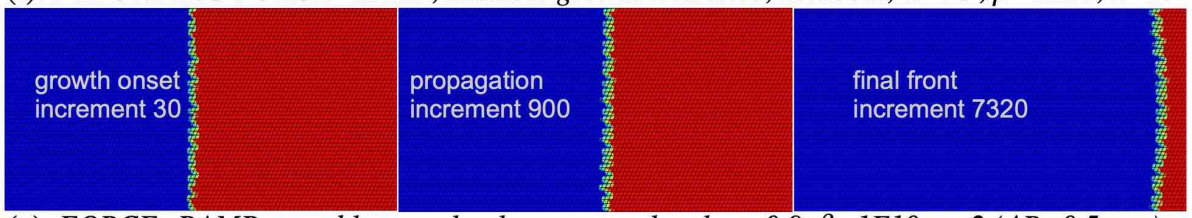

(g). *FORCE=RAMP, unstable growth tolerance, nonlocal, α=0.9, β=1E10, n=2 (ΔB=0.5 mm).*

Figure 32. Delamination front contours during automated VCCT-based propagation analysis obtained from 3D FE models with misaligned meshes (a_0=75mm).